FGI PUBLICATIONS N:O 157

A pipeline of 3D scene reconstruction from point clouds

BY Lingli Zhu

NLS
FINNISH GEOSPATIAL
RESEARCH INSTITUTE
FGI

FGI PUBLICATIONS

N:o 157

A PIPELINE OF 3D SCENE RECONSTRUCTION FROM POINT CLOUDS

by

Lingli Zhu

Doctoral dissertation for the degree of Doctor of Science in Technology to be presented with due permission of the School of Engineering for public examination and debate in Auditorium M1 at the Aalto University School of Engineering (Espoo, Finland) on the 18th of June at 12 noon.

KIRKKONUMMI 2015

Supervising professor
Professor Henrik Haggrén, Aalto University School of Engineering, Department of Real Estate, Planning and Geoinformatics

Thesis advisor
Professor Juha Hyyppä, Finnish Geospatial Research Institute, Department of Remote Sensing and Photogrammetry

Preliminary examiners
Professor Norbert Haala, Stuttgart University, Stuttgart, Germany
Dr. Sander Oude Elberink, University of Twente, Enschede, The Netherlands

Opponent
Professor Stephan Nebiker, University of Applied Sciences Northwestern Switzerland;
Professor Norbert Haala, Stuttgart University, Stuttgart, Germany

ISBN (printed): 978-951-48-0246-1
ISBN (pdf): 978-951-48-0247-8
ISSN (print): 2342-7345
ISSN (online): 2342-7353

Juvenes Print – Suomen Yliopistopaino Oy, Tampere 2015

Aalto University
School of Engineering

Aalto-yliopisto, PL 11000, 00076 AALTO
www.aalto.fi

ABSTRACT

Author
Lingli Zhu

Name of the doctoral dissertation
A Pipeline of 3D Scene Reconstruction from Point Clouds

Unit Department of Real Estate, Planning and Geoinformatics

Publisher Finnish Geospatial Research Institute FGI, National Land Survey of Finland

Series FGI Publications

Field of research Geoinformatics

Manuscript submitted 18 February 2015 **Date of the defence** 18 June 2015

Permission to publish granted (date) 18 May 2015 **Language** English

Article dissertation (summary + original articles)

Abstract

3D technologies are becoming increasingly popular as their applications in industrial, consumer, entertainment, healthcare, education, and governmental increase in number. According to market predictions, the total 3D modeling and mapping market is expected to grow from $1.1 billion in 2013 to $7.7 billion by 2018. Thus, 3D modeling techniques for different data sources are urgently needed.

This thesis addresses techniques for automated point cloud classification and the reconstruction of 3D scenes (including terrain models, 3D buildings and 3D road networks). First, georeferenced binary image processing techniques were developed for various point cloud classifications. Second, robust methods for the pipeline from the original point cloud to 3D model construction were proposed. Third, the reconstruction for the levels of detail (LoDs) of 1-3 (CityGML website) of 3D models was demonstrated. Fourth, different data sources for 3D model reconstruction were studied. The strengths and weaknesses of using the different data sources were addressed. Mobile laser scanning (MLS), unmanned aerial vehicle (UAV) images, airborne laser scanning (ALS), and the Finnish National Land Survey's open geospatial data sources e.g. a topographic database, were employed as test data. Among these data sources, MLS data from three different systems were explored, and three different densities of ALS point clouds (0.8, 8 and 50 points/m^2) were studied.

The results were compared with reference data such as an orthophoto with a ground sample distance of 20cm or measured reference points from existing software to evaluate their quality. The results showed that 74.6% of building roofs were reconstructed with the automated process. The resulting building models provided an average height deviation of 15 cm. A total of 6% of model points had a greater than one-pixel deviation from laser points. A total of 2.5% had a deviation of greater than two pixels. The pixel size was determined by the average distance of input laser points. The 3D roads were reconstructed with an average width deviation of 22 cm and an average height deviation of 14 cm. The results demonstrated that 93.4% of building roofs were correctly classified from sparse ALS and that 93.3% of power line points are detected from the six sets of dense ALS data located in forested areas.

This study demonstrates the operability of 3D model construction for LoDs of 1-3 via the proposed methodologies and datasets. The study is beneficial to future applications, such as 3D-model-based navigation applications, the updating of 2D topographic databases into 3D maps and rapid, large-area 3D scene reconstruction.

Keywords airborne laser scanning, mobile laser scanning, topographic database, building detection, building reconstruction, road detection, road reconstruction

ISBN (printed) 978-951-48-0246-1 **ISBN (pdf)** 978-951-48-0247-8 **ISSN** 2342-7345

Location of publisher Kirkkonummi **Location of printing** Tampere **Year** 2015

Pages: 206 **urn** http://urn.fi/URN:ISBN:978-951-48-0247-8

Aalto-yliopisto
Insinööritieteiden
korkeakoulu

Aalto-yliopisto, PL 11000, 00076 AALTO
www.aalto.fi

Tiivistelmä

Tekijä
Lingli Zhu

Väitöskirjan nimi
Rakennetun ympäristön kolmiulotteinen mallintaminen pistepilvistä

Yksikkö Maankäyttötieteiden laitos

Julkaisija Paikkatietokeskus FGI, Maanmittauslaitos

Sarja FGI Publications

Tutkimusala Geoinformatiikka

Käsikirjoituksen 18.02.2015 **Väitöspäivä** 18.06.2015

Julkaisuluvan myöntämispäivä 18.05.2015 **Kieli** Englanti

Yhdistelmäväitöskirja (yhteenveto-osa + erillisartikkelit)

Tiivistelmä

3D-teknologiat ovat tulleet yhä suosituimmiksi niiden sovellusalojen lisääntyessä teollisuudessa, kuluttajatuotteissa, terveydenhuollossa, koulutuksessa ja hallinnossa. Ennusteiden mukaan 3D-mallinnus- ja -kartoitusmarkkinat kasvavat vuoden 2013 1,1 miljardista dollarista 7,7 miljardiin vuoteen 2018 mennessä. Erilaisia aineistoja käyttäviä 3D-mallinnustekniikoita tarvitaankin yhä enemmän.

Tässä väitöskirjatutkimuksessa kehitettiin automaattisen pistepilviaineiston luokittelutekniikoita ja rekonstruoitiin 3D-ympäristöjä (maanpintamalleja, rakennuksia ja tieverkkoja). Georeferoitujen binääristen kuvien prosessointitekniikoita kehitettiin useiden pilvipisteaineistojen luokitteluun. Työssä esitetään robusteja menetelmiä alkuperäisestä pistepilvestä 3D-malliin eri CityGML-standardin tarkkuustasoilla. Myös eri aineistolähteitä 3D-mallien rekonstruointiin tutkittiin. Eri aineistolähteiden käytön heikkoudet ja vahvuudet analysoitiin. Testiaineistona käytettiin liikkuvalla keilauksella (mobile laser scanning, MLS) ja ilmakeilauksella (airborne laser scanning, ALS) saatua laserkeilausaineistoja, miehittämättömillä lennokeilla (unmanned aerial vehicle, UAV) otettuja kuvia sekä Maanmittauslaitoksen avoimia aineistoja, kuten maastotietokantaa. Liikkuvalla laserkeilauksella kerätyn aineiston osalta tutkimuksessa käytettiin kolmella eri järjestelmällä saatua dataa, ja kolmen eri tarkkuustason (0,8, 8 ja 50 pistettä/m2) ilmalaserkeilausaineistoa.

Tutkimuksessa saatuja tulosten laatua arvioitiin vertaamalla niitä referenssiaineistoon, jona käytettin ortokuvia (GSD 20cm) ja nykyisissä ohjelmistoissa olevia mitattuja referenssipisteitä. 74,6 % rakennusten katoista saatiin rekonstruoitua automaattisella prosessilla. Rakennusmallien korkeuksien keskipoikkeama oli 15 cm. 6 %:lla mallin pisteistä oli yli yhden pikselin poikkeama laseraineiston pisteisiin verrattuna. 2,5 %:lla oli yli kahden pikselin poikkeama. Pikselikoko määriteltiin kahden laserpisteen välimatkan keskiarvona. Rekonstruoitujen teiden leveyden keskipoikkeama oli 22 cm ja korkeuden keskipoikkeama oli 14 cm. Tulokset osoittavat että 93,4 % rakennuksista saatiin luokiteltua oikein harvasta ilmalaserkeilausaineistosta ja 93,3 % sähköjohdoista saatiin havaittua kuudesta tiheästä metsäalueen ilmalaserkeilausaineistosta.

Tutkimus demonstroi 3D-mallin konstruktion toimivuutta tarkkuustasoilla (LoD) 1-3 esitetyillä menetelmillä ja aineistoilla. Tulokset ovat hyödyllisiä kehitettäessä tulevaisuuden sovelluksia, kuten 3D-malleihin perustuvia navigointisovelluksia, topografisten 2D-karttojen ajantasaistamista 3D-kartoiksi, ja nopeaa suurten alueiden 3D-ympäristöjen rekonstruktiota.

Avainsanat ilmalaserkeilaus, liikkuva laserkeilaus, maastotietokanta, rakennusten tunnistus, rakennusten rekonstruktio, tien tunnistus, tien rekonstruktio

ISBN (printed) 978-951-48-0246-1 **ISBN (pdf)** 978-951-48-0247-8 **ISSN** 2342-7345

Julkaisupaikka Kirkkonummi **Painopaikka** Tampere **Vuosi** 2015

Sivumäärä 206 **urn** http://urn.fi/URN:ISBN:978-951-48-0247-8

PREFACE

The study presented in this thesis was carried out as part of my work as a researcher at the Finnish Geospatial Research Institute (FGI), Department of Remote Sensing and Photogrammetry. This thesis has been concentrated on the topic of 3D scene reconstruction from various point clouds. Some automated methods have been developed and implemented to speed up the data processing. The achievement here was a piece of solid work in this topic. In further research work, 3D scene reconstruction will direct to the automation of high detail models from an integration of available resources.

During the past years working in FGI, I would like to say many many thanks to Professor Juha Hyyppä, Head of the Remote Sensing and Photogrammetry Department (FGI): thank him for creating an international environment for us; thank him for his great help and firm support in my research career; thank him for offering me the opportunities of personal development in FGI; also thank him for his inspiring and understanding in some difficult situations. As a head of department, his positive thinking and open-minded communication have created a good atmosphere for our work. Without him, I wouldn't gain today's achievement.

I would extremely thank Professor Henrik Haggren, the supervisor of the thesis, from Aalto University, Department of Real Estate, Planning and Geoinformatics. He was not only as a supervisor of my Doctoral thesis, but also as a supervisor of my Master thesis. Discussions with him have always been valuable. I have learned a lot from him. I would like to specially thank him for his offering me a first job in Finland. And also he has guided me to the research career. Without his help and support, I might not go far in my research career. His encouragement and advices always accompanied me in my late research career.

I would also thank Professor Ruizhi Chen, now Texas A & M University, former head of Navigation and Positioning Department (FGI) (before 2013). I remembered that I was hired by FGI in 2008 because of his coordinated three-year project '3D-NAVI-EXPO'. Since then, '3D' became my oriented research topic. Thank him for bringing me to the '3D world'.

I am thankful to Professor Hannu Hyyppä from Aalto University and Helsinki Metropolia University of Applied Sciences for his support and inspiration in many cooperative projects.

Thanks to the pre-examiners of this dissertation, Professor Norbert Haala, Stuttgart University, and Dr. Sander Oude Elberink, University of Twente, for their efforts and comments. Their comments have brought me for constructive thinking.

I would also express my gratitude to all colleagues for bringing me a harmonious working atmosphere. Especially, the co-authors of the appended papers, Antero Kukko, Anttoni Jaakkola, Harri Kaartinen, Matti Lehtomäki, and Anssi Krooks have given great support in this study. I would also like to thank Leena matikainen, Tuomas Turppa, Eero Salminen and Yiwu Wang for their support and cooperation. I am also thankful to Heli Honkanen for her help in translating the abstract of this thesis into Finnish during the late stage of my thesis. It has been a pleasant experience to work with them all.

This thesis will be the first one in using a new designed cover after the FGI merging to the National Land Survey of Finland (NLS). Thanks Professor Tiina Sarjakoski, Research Director of FGI, for her arrangement to make things go smoothly in a new system.

With our Chinese colleagues in FGI, I enjoyed the lunch time with them. They have brought happy and joyful time for me. Nice to meet them in Finland!

Many thanks to my friends and my families. Because of them, my life became wonderful. Thank them all for their sustained support, care and love!

Kirkkonummi, 6 May 2015

Lingli Zhu

CONTENTS

List of the publications

The thesis consists of a summary and the following publications, which are referred to in the text by their Roman numerals:

I. **Zhu, L.**, Hyyppä, J., Kukko, A., Kaartinen, H. and Chen, R., 2011. Photorealistic Building Reconstruction from Mobile Laser Scanning Data, *Remote Sens.*, 2011, *3*(7), 1406-1426; doi:10.3390/rs3071406.

II. **Zhu, L.**, Hyyppä, J., 2014. The Use of Airborne and Mobile Laser Scanning for Modelling Railway Environments in 3D. *Remote Sens.*, 2014, 6(4), 3075-3100; doi:10.3390/rs6043075.

III. **Zhu, L.**, Jaakkola, A., Hyyppä, J., 2013. The use of Mobile Laser Scanning data and Unmanned Aerial Vehicle images for 3D model reconstruction. *International Archives of the Photogrammetry, Remote Sensing and Spatial Information Sciences*, Volume XL-1/W2, 2013, UAV-g2013, 4 – 6 September 2013, Rostock, Germany.

IV. **Zhu, L.**, Lehtomäki, M., Hyyppä, J., Puttonen, E., Krooks, A., Hyyppä, H., 2015. Automated 3D Scene Reconstruction from Open Geospatial Data Sources: Airborne Laser Scanning and a 2D Topographic Database. *Remote Sens.*, 7(6), 6710-6740; doi:10.3390/rs70606710.

V. **Zhu, L.**, Hyyppä, J., 2014. Fully automated power line extraction from airborne laser scanning point clouds in forest areas, *Remote Sens.* 2014, *6*(11), 11267-11282; doi:10.3390/rs61111267.

VI. Hyyppä, J., **Zhu, L.**, Liu, Z., Kaartinen, H., Jaakkola, A., 2012. (Eds.), Ubiquitous positioning and mobile location-based services in smart phones: 3D City Modeling and Visualization for Smart Phone Applications (chapter 10), Copyright © 2012 by IGI Global, ISBN 978-1-4666-1827-5.

III is a peer-reviewed conference article. **VI** is a peer-reviewed book chapter. Other publications are peer-reviewed journal articles listed in Core Collection Articles of ISI Web of Science Core Collection.

.

The author's contribution

In **I**, I performed the method development, testing and paper writing. Juha Hyyppä was the advisor in the study, and he participated in project planning. Antero Kukko and Harri Kaartinen were responsible for data acquisition. Ruizhi Chen was the project supervisor.

In **II**, I was responsible for the method development, testing and paper writing. Juha Hyyppä supervised the writing and participated in project planning.

In **III**, I was responsible for the method development, testing and paper writing. Anttoni Jaakkola was responsible for data acquisition. Juha Hyyppä was the project supervisor.

In **IV**, I was responsible for planning, development and writing. Matti Lehtomäki developed the method for plane detection and evaluated the plane detection result. Juha Hyyppä was the project supervisor. Eetu Puttonen participated in a minor part of the development. Anssi Krooks prepared the materials. Hannu Hyyppä was also the project supervisor.

In **V**, I was responsible for the method development, testing and paper writing. Juha Hyyppä was the project supervisor, and he participated in project planning.

In **VI**, I was a co-author, planned the study, prepared the article and participated in writing. Prof. Juha Hyyppä was the author responsible for writing the paper. Zhengjun Liu, Harri Kaartinen and Anttoni Jaakkola provided parts of the materials.

List of Abbreviations

LS	Laser scanning
ALS	Airborne Laser Scanning
CAD	Computer-aided Design
MLS	Mobile Laser Scanning
TLS	Terrestrial Laser Scanning
GPS	Global Positioning System
IMU	Inertial Measurement Unit
INS	Inertial Navigation System
DEM	Digital Elevation Model
DTM	Digital Terrain Model
FGI	Finnish Geodetic Institute
NLS	National Land Survey
3D	Three-dimensional
LiDAR	Light Detection and Ranging
TIN	Triangulation irregulated network
LoD	Level of Detail
RANSAC	Random sample consensus

1. INTRODUCTION

1.1 Background and motivation

3D modeling is the process of forming the 3D surface of an object. The result is a 3D model. A 3D model is formed from a set of vertices that define the shape of the object. Recently, the technologies for 3D modeling have been gaining popularity in industrial, consumer, entertainment, healthcare, education, and governmental applications. According to a market research report (Market research report, 2014, online), the 3D modeling and mapping markets are expected to grow from $1.1 billion in 2013 to $7.7 billion by 2018. Smartphone companies, such as Google, Microsoft, Apple, and Samsung, have shown substantial interest in 3D map applications. 3D maps have numerous advantages compared to 2D maps, including facilitating better navigation, decision making and information visualization in urban planning, in many general smart city concepts, and location-based services. 3D modeling solutions enable users to rapidly construct 3D maps of surrounding areas.

Major data sources used in 3D modeling include photogrammetric images, laser scanning (LS) and existing map data. Photogrammetry is the technology of deriving 3D data from 2D images by mono-plotting (single-ray back projection), by stereo-imagery interpretation or by multi-image block adjustment. In the past, photogrammetry played a major role in the derivation of geographic data. The current technology in LS offers an alternative solution for the acquisition of 3D geographic data (Hyyppä et al., 2008). LS is based on laser (LIDAR) range measurements from a carrying platform and on the precise positioning and orientation of the platform. LS is also referred to as Light Detection and Ranging (LIDAR) because it uses a laser to illuminate Earth's surface and a photodiode to register the backscatter radiation. The time it takes for the laser beam to reach the target and return to the source (delay) is used to measure the distance to the target, i.e., with the speed of light. After GPS, IMU, and scanning mechanisms were attached to laser ranging measurement devices, initially for military purposes in the 1980s and later for surveying purposes, the field of science currently known as airborne LS (ALS) was born. The typical operating wavelength range used in LIDAR is between 250 and 1,600 nm, and the most commonly used wavelengths in LS are close to 1,000 nm, i.e., 905 or 1,064 nm. However, these wavelengths are easily absorbed by the eye. An alternative laser with a 1,550 nm wavelength is safe for eyes at higher power levels. Based on the development of electro-optical sensor technology together with the development of direct geo-referencing methods since the mid-1990s, airborne LS integrated with GPS and IMU has become available (Petrie, 2010) for direct 3D data acquisition. Significant advancements over nearly two decades have resulted in the current situation, whereby LIDAR systems have become important sources of high-resolution and accurate 3D geographic data (Toth, 2009). Currently, ALS systems are extremely practical solutions for mapping large areas with a high degree of accuracy, e.g., to determine elevations and generate 3D models. Elevation accuracies of 5-10 cm are common, whereas planimetric accuracies range between 20 and 80 cm, depending on the flying height and IMU characteristics (Hyyppä et al., 2009). The planimetric error of the just-announced Optech TITAN is 1/7500 times the height [m], i.e. less than 30 cm from an altitude of 2 km. The density of point collection has been greatly improved after a decade's worth of development. For instance, in 1993, the pulse repetition frequency (PRF) of ALS was 2 kHz, whereas in 2013, it had increased to 800 kHz. The point density has increased from a few points per square meter to the current density of 50 points/m^2.

Mobile LS (MLS), which is also called mobile terrestrial LS, is currently a rapidly developing area in LS, with laser scanners, GNSS and IMU being mounted onboard moving vehicles. MLS can be considered to fill the gap between ALS and terrestrial LS (TLS). In MLS, data collection can be performed either in the so-called stop-and-go mode or in a continuous mode. The stop-and-go mode corresponds to conventional TLS measurements; therefore, MLS is hereafter used to refer to the continuous model, i.e., the use of continuous scanning measurements along the drive track. In addition to laser scanners, MLS data acquisition sensors can include accessories, such as digital cameras thermal camera, spectrometers and video cameras. The past few years have seen remarkable development in MLS to accommodate the need for large-area and high-resolution 3D data acquisition. MLS serves one of the fastest growing market segments: 3D city modeling (Toth, 2009). Advanced real-time visualization for location-based systems, such as vehicle navigation (Cornelis et al., 2008) and mobile phone navigation (Chen et al., 2010), require the large-scale 3D reconstructions of street scenes. The use of MLS results in different point densities and greater scanning angles and closer ranges to the objects compared to ALS. State-of-the-art MLS has a scan rate of 400 lines per second; the MLS RIEGL VMX-450-RAIL (RIEGL, USA) can measure up to 1.1 million points per second along the trajectory of a moving platform with a 360° field of view without gaps (RIEGL website, USA, 2014, online). The measurement distance to the objects can range from 0.3 to 800 m. The development of mobile sensor technology has made it possible to acquire data from complex terrains and scenes because of its use of various flexible platforms, such as aircraft, cars or van, trains, boats, trolleys and personal backpacks. An example of MLS used for surveying applications in the field of natural sciences can be found in Kukko et al. (2012).

Unmanned aerial vehicles (UAVs) were originally used for target practice to train military personnel. UAVs are becoming standard platforms for the large-scale mapping of areas of limited extent (Haala et al., 2013). Low-cost UAVs with a camera, a laser scanner or both are widely utilized for surveys. The main reasons are the following: i) survey cost considerations; ii) the safety factor, whereby the lack of a pilot makes it convenient to collect data in disaster areas, e.g., areas affected by floods, earthquakes and tsunamis; iii) low-altitude data acquisition, which fills the gap between high-altitude flight observations and close-range ground-based observations; iv) and their ability to perform data acquisition of locations where MLS cannot observe. Typically, camera-based UAVs collect images with large overlaps. Dense point clouds can be generated from such images. The quality of 3D point clouds from UAV images was discussed by Haala et al. (2013).

Open geospatial data have gained considerable popularity in the past few years. Various national governments have provided geospatial data as open data sources on websites to share and explore the potential of data through the development of applications to address public and private demands. In the spring of 2010, the UK government allowed a significant number of datasets to be freely accessible by the general public via a program named ShareGeo Open (ShareGeo Open repository, 2014, online). These datasets included many core datasets held by the Office of National Statistics, the Central Government and the Ordinance Survey. Since May 1, 2012, the Finnish NLS has made its topographic datasets freely available to the public. According to the NLS's agreement, the open data product can be used without compensation and with extensive and permanent rights of use (NLS website, 2014, online). In March 2014, the commercial software company Esri launched the ArcGIS Open Data site, which enables organizations to create custom open data websites. As more open geospatial databases become available, the trend to update the geospatial databases from 2D to 3D became evident due to the increasing need for 3D applications, such as flood risk modeling, flight path planning, and environment and

coastal protection. In 2012, the Netherlands established the 3D national standard for large-scale topography (Geospatial world forum, 2012). In December 2013, Singapore launched a plan for the development and maintenance of a 3D topographic database. In Finland, the need to update a 2D topographic database to a 3D topographic database is urgent because ALS data continuously proliferate throughout Finland. Therefore, one of our motivations in this thesis was to investigate the NLS 2D topographic database and to advance the technology for updating 2D topographic databases to 3D.

The available resources have provided support for our 3D modeling study. This thesis will address the method development based on these sources for automated 3D object detection and 3D model reconstruction.

1.2 Hypothesis

This study is based on the following hypotheses:

- 3D scene (including terrain, buildings and roads) can be reconstructed from point clouds and topographic databases by developing automated methods and that these methods can produce good results.
- Object classification (e.g. buildings and power lines) approaches for ALS can be automated.

1.3 Objectives of the study

The objectives of this study is to develop techniques for 3D modelling using various data sets such as from ALS, MLS, UAV images and topographic database data. The sub-objectives are as follows:

i) Develop an automated pipeline from original point clouds to 3D model reconstruction;

ii) Develop approaches for various point cloud classification schemes;

iii) Reconstruct different LoDs of 3D models;

iv) Explore different data sources for 3D model reconstruction; and

v) Evaluate the accuracy of the methods and the operability in practice.

1.4 Structure and contribution of the study

The thesis consists of a summary and six original publications. In addition to the background and introduction, in the summary section, various previous studies will be addressed, the developed methods will be presented, the results will be demonstrated, and future considerations will be discussed.

To achieve the above objectives, the following research has been performed:

- Paper **I** presents the procedure of photorealistic 3D building model reconstruction from MLS point clouds and terrestrial images. In this paper, the author investigates the feasibility of using MLS data for building reconstruction. The findings indicate that when MLS data around the buildings are available and when the building roofs are flat, the building models can be reconstructed using MLS data. The methods for ground and building classification, plane detection, texture acquisition and mapping are addressed. This study provides new information for the use of MLS data.
- Paper **II** introduces the 3D railway environment reconstruction from ALS and MLS. In this study, multiple algorithms, from object classification to 3D visualization, were developed to provide object extraction from ALS and ground model simplification. The strengths and weaknesses of the object extraction from ALS and MLS were addressed. The findings indicated that the ground and building roof extraction from ALS exhibited considerable advantages, and the building walls and poles from MLS exhibited advantages. Either ALS or MLS can be utilized for power lines. However, this choice

heavily depends on the scene situation, availability of data and density of ALS point clouds.

- Paper **III** addresses the use of MLS and UAV images for 3D model reconstruction. The study indicates that MLS data and UAV images have complementary characteristics. Camera-based UAVs can not only provide information from a top view but also offer useful data for areas in which MLS platforms are not accessible, such as various private yards and certain small tracks. In this paper, registration between MLS and UAV images was considered. The poles from MLS were utilized to register the datasets in a consistent coordinate system. Thus, a complete model was obtained.
- Paper **IV** develops automated 3D scene reconstruction from ALS and a topographic database. The focus of this study is on automated algorithm development for 3D building models and 3D road network reconstruction from ALS and Finnish National Land Survey (NLS) open geospatial datasets. The motivation was to investigate the open geospatial database from the NLS and to advance the technology for updating 2D topographic databases to 3D. As a result, a 3D scene consisting of a 3D terrain model, 3D building models and 3D road networks was automatically reconstructed.
- Paper **V** proposes a robust approach for power line extraction from high-density ALS in forested areas. Our method was developed based on a statistical analysis and 2D image-based processing technology. This method was performed using six sets of ALS data from different forest environments. A comparison with reference data indicated that 93.26% of power line points were correctly classified. This approach can also be used in urban and open areas.
- Paper **VI** is a book chapter. This book chapter contains a detailed review of data acquisition, object classification, 3D reconstruction and 3D visualization. 3D city modeling for mobile-phone-based applications is emphasized.

2. LITERATURE REVIEW

In the past two decades, various studies on point cloud classification and 3D object reconstruction have made considerable progress. Numerous methods have been proposed in the photogrammetry, remote sensing and computer vision fields. The following section reviews methods in object detection and 3D model reconstruction from point clouds.

2.1 Object detection from LS data

Methods for object detection rely heavily on data sources. Data from the field of photogrammetry, such as single images, stereo images or multiple images, are used to extract edge features or line-shaped objects, which provides significant benefits. However, planar feature extraction often relies on texture recognition, which is considerably influenced by an object's reflection, the light source, the angle of illumination, and the position of the camera. Therefore, it is more reliable to acquire planar features from laser point clouds (Kaartinen and Hyyppä, 2006). A georeferenced LS point cloud includes, broadly speaking, coordinates, echoes, reflectance, and time information, which are used in the classification. Statistical classification methods are commonly used. Points can be divided into various classes using intensity values, echoes (e.g., only, the first of many, intermediate or last pulse), and height and location information. The heights can be relative to the ground, or they can be absolute values. Various filtering techniques have been developed for applications, such as ground classification, building, road and power line extraction.

The approaches for the classification of ground points from laser point clouds have been proposed by various researchers, including Arefi and Hahn (2005), Axelsson (2000),

Fowler et al. (2006), Kobler et al. (2007), Kraus and Pfeifer (1998), Liang et al. (2014), Meng et al. (2009), Mongus et al. (2014), and Wack and Wimmer (2002). Kraus and Pfeifer (1998) developed a DTM algorithm for wooded areas. The terrain points and non-terrain points were distinguished using an iterative prediction of the DTM and weights attached to each laser point based on the vertical distance between the expected DTM level and corresponding laser point. Axelsson (2000) developed a progressive TIN densification method that is implemented in the TerraScan software (Terrasolid, Finland). A comparison of the filtering techniques used for DTM extraction can be found in a report on an ISPRS comparison of filters (Sithole and Vosselman, 2004). The results validated that all filters exhibited good performance on smooth rural landscapes but that errors were produced in complex urban areas and rough terrain with vegetation. Meng et al. (2010) investigated state-of-the-art ground filtering techniques. The authors noted that ground filters commonly utilized four characteristics: lowest feature in a specific area, ground slope threshold, ground surface elevation difference threshold, and smoothness. Slope-based and direction-based techniques were widely applied. Ground filtering for rough terrain or discontinuous slope surfaces, dense forest canopies and low vegetation areas remain challenging (Meng et al., 2010). After ground point classification, it is important to simplify the ground model for, e.g., visualization, rendering, and animation. A few methods for terrain simplification have been addressed by, e.g., Ben-Moshe et al. (2002) and Gu et al. (2014). To speed up data visualization, most methods were designed to improve the performance of data processing (e.g., optimizing the efficiency of fetching and accessing data) instead of reducing data, for example, using an out-of-core algorithm.

Regarding classification of building points from ALS, previous research has shown that buildings can be automatically detected from ALS data with relatively high accuracy (e.g., Awrangjeb et al. (2012, 2014); Belgiu et al., 2014; Chen et al., 2012; Chen at al., 2014; Dorninger and Pfeifer, 2008; Forlani et al., 2006; He et al., 2014; Karsli and Kahya, 2012; Liu et al., 2012; Matikainen et al., 2003; Melzer, 2007; Mongus et al., 2014; Moussa and El-Sheimy, 2012; Niemeyer et al., 2011; Rottensteiner et al. (2005b, 2012, 2013, 2014), Tournaire et al., 2010; Vögtle and Steinle, 2003; Verma et al., 2006; Vosselman et al. 2004; Waldhauser et al. 2014; Zhang et al. 2006; Rutzinger et al., 2009; Yang et al., 2014). Different types of features, including local co-planarity, height texture or surface roughness, reflectance information from the images or from LS data, height differences between the first pulse and last pulse of laser scanner data, and shapes and sizes of objects, have been used to separate buildings and vegetation. State-of-the-art building detection information can be found in the latest results from ISPRS benchmarks in urban object detection and 3D building reconstruction. This benchmarks were launched in 2012. The results were published in July 2014 (Rottensteiner et al., 2014). In this benchmark, two test areas with five datasets were provided. The first test contained georeferenced 8-cm GSD aerial color infrared images with 65% forward overlap and 60% side overlap and an ALS with a density of 4-7 points/m^2 from an area in Vaihingen, Germany. The second test contained a set of georeferenced 15-cm GSD RGB color images with 60% forward overlap and 30% side overlap and ALS data with a density of approximately 6 points/m^2 from an area in Vaihingen, Germany. Rottensteiner et al. (2014) discussed the results from this campaign. There were 27 methods presented in their study. The methods were divided into three groups: supervised classification, predominated model-based classification and heuristic models based on statistical sampling for the energy functions. The latter two did not include training datasets and thus can be classified as unsupervised methods. The evaluation of the detected results was based on all buildings and only on buildings larger than 50 m^2. The results from detecting buildings larger than 50 m^2 were promising.

However, detecting small buildings and separating trees from roofs continued to present challenges. There remains room for improvement.

In recent years, object modelling from MLS has become a focus of researchers. The applications typically consisted of extracting building walls, poles, road marks, power lines and other city furniture such as traffic signs and streetlights. The studies have been addressed in Brenner (2009), Cornelis et al. (2008), Guan et al. (2014), Jaakkola et al. (2008, 2010); Jochem et al. (2011), Lehtomaki et al. (2010), Toth (2009), Pu et al. (2011), Yang et al. (2013, 2015), and Zhao and Shibasaki (2003, 2005). Early studies from Zhao et al. (2003) have proposed a fully automated method for reconstructing a textured CAD model of an urban environment using a vehicle-based system equipped with a single-row laser scanner and six line cameras plus a GPS/INS/Odometer-based navigation system. The laser points were classified into buildings, ground and trees by segmenting each range scan line into line segments and then grouping the points hierarchically. The vertical building surfaces were extracted using Z-images, which were generated by projecting a point cloud onto a horizontal (X-Y) plane, where the value of each pixel in the Z-image is the number of the point cloud falling on the pixel. However, for a single building, the Z-image is not continuous in intensity as a result of the windows in the walls. Therefore, this method is not so useful when addressing buildings with large reflective areas, e.g., balconies with glass or windows. Additionally, problems related to object occlusion have been reported. The latest study on MLS classification was performed by Yang et al. (2015). The authors presented an approach based on multi-scale super-voxel segmentation for MLS point cloud classification. Consequently, buildings, street lights, trees, telegraph poles, traffic signs and cars were classified from MLS data with an overall accuracy of 92.3%.

The available approaches for extracting power lines from ALS are described in Melzer and Briese (2004), Clode and Rottensteiner (2005), McLaughlin (2006), Jwa et al. (2009), Kim and Sohn (2011, 2013), and Sohn et al. (2012). Melzer and Briese (2004) proposed a method for power line extraction and modeling via ALS using a 2D Hough transformation and 3D fitting methods. Jwa (2009) introduced a voxel-based piecewise line detector (VPLD) approach for automated power line reconstruction using ALS data. This method was based on certain assumptions, such as the transmission line not being disconnected within one span and the direction of the power line not changing abruptly within a span. The latest contribution to power line classification and reconstruction using ALS data was by Sohn et al. (2012) and Kim and Sohn (2013); Sohn et al. used a Markov random field (MRF) classifier to discern the spatial context of linear and planar features, such as in a graphical model for power line and building classification. They assumed that power lines run through inhabited areas with many buildings. Power line pylons were classified and indicated the connection between power lines. Kim and Sohn (2013) proposed a point-based supervised random forest method for five utility corridor object classifications from an ALS point cloud set with a density of 25-30 points/m^2. Based on the above literature review, the methods for power line detection can be summarized into two types: line-shape-based detection methods (e.g., RANSAC and 2D Hough transformation (Axelsson, 1999; Melzer and Briese, 2004; Liu et al., 2009; Liang et al., 2011; Li et al., 2010)) and supervised classification methods (McLaughlin, 2006; Jwa et al., 2009; Kim and Sohn, 2011; Sohn et al., 2012).

2.2 Object reconstruction

3D reconstruction is the process of determining the shape and appearance of objects. 3D building reconstruction from airborne-based data, including ALS and images, significant efforts have been made by many researchers, e.g., Vosselman, et al. (1999, 2001, 2002, 2010), Brenner, et al. (1998, 2000, 2004, 2005), Haala et al. (1998, 1999, 2004, 2006,

2010), Rottensteiner et al. (2003, 2005b, 2012, 2013, 2014), and Elberink (2006, 2008, 2009, 2010, 2011). In addition, more recent studies on building reconstruction have been presented by Bulatov et al. (2014), Hron and Halounová (2015), Huang et al. (2013), Jochem et al. (2012), Kim and Shan (2011), Perera et al. (2014), Rau and Lin (2011), Sampath and Shan (2010), Seo et al. (2014), Xiong et al. (2014), Yan et al. (2015), and Zhang et al. (2011).

Vosselman (1999) proposed a building reconstruction method using ALS data. The roof patches were segmented using a 3D Hough transformation. The edges are identified using the intersection of faces and an analysis of height discontinuities. The roof topology is built by bridging the gaps in the detected edges. The use of geometric constraints is proposed to enforce building regularities. In a subsequent approach (Vosselman and Dijkman, 2001; Vosselman and Süveg, 2001), ground plans are used. If building outlines are not available, they are manually drawn in a display of the laser points with color-coded heights. The concave ground plan corners are extended to cut the building area into smaller regions, and Hough-based plane extraction is constrained to these regions. Split-and-merge is used to obtain the final face. To preserve additional details in the model, another reconstruction method, a model-driven approach, has been explored. Building models were interactively decomposed to meet the predefined simple roof shape (flat, shed, gable, hip, gambrel, spherical, or cylindrical roof).

The approach of Brenner and Haala (1998) uses DSMs and 2D ground plans as data sources in an automatic and/or semiautomatic reconstruction process. First, ground plans are divided into rectangular primitives using a heuristic algorithm. For each of the 2D primitives, a number of different 3D parametric primitives from a fixed set of standard types are instantiated, and their optimal parameters are estimated. The best instantiation is selected based on area and slope thresholds and on the final fit error. The 3D primitive selection and parameters can be later modified using a semiautomatic extension. A human operator can use aerial images to refine the automatic reconstruction when semi-automatic post-processing is performed. Rectangles of ground plan decomposition can be interactively modified or added, and these rectangles are again used for 3D primitive matching. This interactive mode can also be used if no ground plan is available. The final object representation is obtained by merging all 3D primitives. Brenner (2000b) uses regularized DSM and ground planes for building-model reconstruction. A random sampling consensus (Fischler and Bolles, 1981) was applied for roof plane detection. A set of rules expressing possible labeling sequences, i.e., possible relationships between faces and the ground plan edges, is used to either accept or reject the extracted face. Regularity is enforced using additional constraints and least squares adjustment.

Haala and Brenner (1999) used laser scanning data and ground plans for building reconstruction. The first step was to acquire DSM from laser point cloud data. Then, DSM was simplified to reduce the number of presented points. Next, the ground plan was decomposed according to the DSM normal. An interactive editing tool was developed to refine the initial reconstruction. Finally, 3D CAD models were reconstructed. Terrestrial images were used for photorealistic building facades. In a subsequent approach by Haala et al. (2006), the authors presented a cell decomposition method for both roof and facade reconstruction from input data of ground plans, ALS and TLS. This approach provided greater performance for building model reconstruction at different scales.

Rottensteiner and Briese (2003) used laser data (for regularized DSM) and aerial images (to perform segmentation of aerial image grey levels and expansion by region-growing algorithms). In this method, planar roof segments are detected using the DSM normal vectors integrated with the segments from the aerial images. Plane intersections and step edges are detected, and a polyhedral model is derived. Rottensteiner et al. (2005a) only

used laser data. Roof planes were detected using the surface normal vectors. The detection of plane intersects and step edges was then performed. Finally, all step edges and intersection lines were combined to form the polyhedral models. The author's recent contributions to the ISPRS benchmark for urban object detection and 3D building reconstruction can be found from Rottensteiner et al. (2012, 2013, and 2014). More information about the ISPRS benchmark will be introduced later.

Elberink (2008) noted problems in using dense ALS data for automated building reconstruction and also discussed problems in model-driven methods and the combination of data- and model-driven approaches. Specifically, the following problems were noted: uneven distribution of the laser points; the determination of the parameters for roof plane segmentation; inconsistencies between point clouds and ground plans when using ground plans; misclassification or incompleteness of laser point data when not using ground plans; errors from building outline detection due to the missing laser points; creating hypotheses about 3D building shapes; challenges in reconstructing complex building shapes and certain small details when using model-driven methods; and conflicts when applying the thresholds for the final shape of the model when using a combination of data- and model-driven approaches. In Elberink (2009), the author developed a target-based graph matching approach for building reconstruction from both complete and incomplete laser data. The method was validated using test data from residential areas of Dutch cities characterized by architectural styles consisting of villas and apartment houses. Of 728 buildings, 72% exhibited complete shape matching, 20% resulted in incomplete matches, and 8% failed to fit to the initial laser points.

The reviews of building reconstruction methods can be found in, e.g., Brenner (2005), Kaartinen and Hyyppä (2006), Haala and Kada (2010), Rottensteiner et al. (2012, 2013, 2014). Brenner (2005) investigated reconstruction approaches based on different automation levels, in which the data were provided by airborne systems, and Kaartinen and Hyyppä (2006) collected building extraction methods from eleven research agencies in four testing areas. The input data contain airborne-based data and ground plans (for selected buildings). Building extraction methods were analyzed and evaluated from the aspects of the time consumed, the level of automation, the level of detail, the geometric accuracy, the total relative building area and the shape dissimilarity. Haala and Kada (2010) reviewed building reconstruction approaches according to building roofs and building facades, in which the input data covered both airborne- and ground-based data. The approaches related to building reconstruction can be grouped into three categories: data-driven, model-driven and a combination of data- and model-driven approaches. Haala and Kada (2010) classified the building reconstruction methods into three types: i) reconstruction with parametric shapes, ii) reconstruction with segmentation, and iii) reconstruction with digital surface model (DSM) simplification. Methods in the first category are model-driven methods, whereas methods in the latter two categories are data-driven methods. The strengths and weaknesses of the data- and model-driven methods have been discussed in previous studies (Tarsha-kurdi, 2007). For example, data-driven methods are more flexible and do not require prior knowledge; however, the density of the data has a significant effect on the resulting models. Model-driven approaches predefine parametric shapes or primitives, such as simple roof prototypes (e.g., gable, hip, gambrel, mansard, shed and dormer). Building models can be reconstructed by using a combination of different primitives. One of the advantages of a model-driven approach is that a complete building roof model can be constructed according to predefined shapes when some building roof data are missing (e.g., due to reflection or an obstacle). However, failure is possible when reconstructing complex buildings and building models that are excluded in predefined shapes (Haala and Kada, 2010).

The results of building reconstruction using ISPRS benchmarks for urban object detection and 3D building reconstruction performed in 2012 can be found in Rottensteiner (2014). Fourteen different building reconstruction methods were submitted. Ten methods were based on ALS points, two methods employed images, one method was based on a raster DSM from ALS, and one method used both images and ALS data. The results indicated that ALS data were preferred to images during building reconstruction. Eight methods were based on generic building models, five methods were employed adaptive predefined models, and one method was based on primitives. Data-driven methods are more prevalent in this benchmark. During the reconstruction process, under-segmentation was the dominant error type for areas with small buildings, whereas over-segmentation errors were common for areas with large roofs. From this study, the authors noted that further improvement of the reconstruction of small buildings and complex flat roofs was needed (Rottensteiner, 2014).

The challenges of building reconstruction have been addressed in previous research. For example, Elberink (2010) presented promising methods utilizing both model-driven and data-driven approaches for oblique roof reconstruction. However, the author noted that reconstruction was not feasible when buildings contain complex height jumps and flat roofs because the proposed algorithm could not reliably locate all edges of flat roof segments and because the locations of corner points inside the polygon were not detected (Elberink, 2010). In addition, the results from ISPRS benchmark (Rottensteiner, 2014) also evidenced that reconstruction of complex flat roofs was still a challenging work. In this thesis, the solutions to the problems will be addressed.

In regard to road modeling, Mayer et al. (2006) addressed the results of road extraction from the EuroSDR benchmark campaign. Eight test images from different aerial and satellite sensors were used. The results showed that with limited complexity, it was possible to extract roads with high quality in terms of completeness and correctness. Many studies have provided evidence that an ALS point cloud is suitable for road detection and reconstruction. Vosselman (2003) used ALS and 2D information from cadastral maps to model the surfaces of streets. Clode et al. (2007) proposed a method for classifying roads using both the intensity and range of LIDAR data. Elberink (2010) employed road vectors (road edges) from a topographic database and obtained the heights via ALS for 3D road network generation. Beger et al. (2011) utilized high-resolution aerial imagery and laser scanning data for road central line extraction. Boyko and Funkhouser (2011) utilized a road map and a large-scale unstructured 3D point cloud for 3D road reconstruction. Although certain studies on 3D road modeling have been implemented, room for improvement remains in terms of differences amongst applied data sources. In this thesis, we not only developed approaches tailored to upgrading 2D roads (with central lines of carriageways) from the NLS topographic database to 3D road models (with road edges and heights) but also investigated the availability of ALS point clouds of different densities for 3D road reconstruction.

3. MATERIALS AND METHODS

3.1 Study areas and materials

A summary of the study areas used in **I-V** is presented in Table 1. Table 2 summarizes the datasets used in the study. Further details of the datasets and their applications can be found in **I-V**, and the references are listed in Table 1 and Table 2. Publication **VI** consisted of a review of data acquisition, object detection and reconstruction methods; current

applications; freely available sources; and a case study. Therefore, **VI** is not included in Table 1 and Table 2.

Table 1. Study areas and materials.

Publication	Study area	Description of study area
I	Tapiola downtown, Espoo	An area of commercial buildings, including shopping centers, banks, government agencies, bookstores, and high-rise residential buildings, with the tallest building being 45 m in height.
II	Kokemäki railway station and its surroundings, Kokemäki	A railway environment, including the ground, railroads, buildings, high voltage power lines, pylons.
III	Sundsberg area, Espoo	This area included various stylish buildings. The poles were placed on the sides of the roads.
IV	A 6*6 km area with the lower left corner (374000, 6672000), Espoo.	A part of Espoo city, including various buildings and roads as well as terrain with small height variations.
V	Forest areas in Kirkkonummi	Forest areas containing power lines.

Table 2. Summary of the datasets.

Paper	Data used in the study	Original data source	Purpose of use
I	MLS point clouds with corresponding georeferenced 3D coordinates, GPS time, profile info, and position and orientation of the MLS system. The point cloud coordinates were in a map coordinate system (ETRS-TM35FIN with GRS80 ellipsoidal height)	MLS data were collected by the FGI ROAMER system (using the Faro Photon^{TM} 120 laser scanner) mounted on a trolley (Kukko, 2009). The data was collected on the 12th of May, 2010.	The MLS point cloud was utilized for ground and building extraction and 3D building reconstruction. The position and orientation information of the MLS system were applied for point cloud noise removal.
I	Terrestrial images were manually captured according to the building texture requirements	Images were taken by a Canon EOS 400D digital camera.	These images were applied as building textures. In addition, these images were also used for interactively checking the building geometry.
I	Reference aerial images	Bing maps produced by Microsoft	Interactive checking of reconstructed buildings for quality control

II	ALS point cloud with georeferenced 3D coordinates. The density of the point cloud was 49.62 points/ m^2.	The ALS data were acquired at an altitude of 300 m with a Topeye system (S/N 742) on a helicopter platform.	Ground, building roof and power line extraction
II	MLS point cloud with georeferenced 3D coordinates. After data cleaning and thinning were performed, the average point density was 720 points per m^2.	StreetMapper mobile mapping system composed of two Riegl VQ250 scanners, DGPS and IMU components. This system was mounted on a train wagon for data collection.	Building facade and pole detection
II	Orthophoto with a ground resolution of 20 cm	Orthophoto was derived from the DEM and aerial images taken by a Rollei camera with a resolution of 7816*5412 pixels.	Reference data for building and power line quality evaluation
III	MLS point cloud with georeferenced 3D coordinates, pulse width, profile number, echo number, time stamp for the point and the profile	FGI Sensei mobile mapping system consisting of Ibeo Lux scanner, GPS and IMU, which was mounted on a car.	Building facade and pole detection
III	UAV images with RGB channels	FGI camera-based UAV system consisting of a quadrocopter type Microdrone md4-200 UAV and a Ricoh GR Digital II low-cost RGB compact camera.	Image bundle block adjustment and building roof extraction
III	Control points	The positions of the poles from MLS were applied as control points.	UAV image georeferencing
IV	ALS point cloud with a density of 0.8 points per square meter and laser echo information in the ETRS-TM35FIN coordinate system	NLS open data sources.	Building geometry model reconstruction and road height information derivation
IV	ALS point cloud with a density of 8 points per square meter in the ETRS-TM35FIN coordinate system	ALS datasets were provided by the municipality of Espoo.	Road edges and height information extraction

IV	Road carriageway central line and its 'Class' information	Topographic database	3D road reconstruction
IV	Orthophoto	NLS open data sources	Ground texture
IV	236 referenced roof segments	Orthophoto and original ALS point cloud	Evaluate the correctness of planar detection
IV	15 reference heights in building test area	ALS point cloud with 0.8 points per square meter	Evaluate the height accuracy of building models
IV	Eight road reference datasets including road width and height data	ALS point cloud with 8 points per square meter	Quality evaluation of 3D road models
V	Six sets of ALS point clouds with georeferenced 3D coordinates and a density of 55 points per square meter	All ALS datasets were collected from Kirkkonummi, Finland	Power line classification
V	Referenced power line points	Reference data were manually obtained using Terrascan software (Terrasolid, Finland)	Quality evaluation of power line extraction

3.2 Methods for quality evaluation

The quality of the results in **II**, **III** and **V** was evaluated by comparing the results to the reference data. The reference data were interactively acquired from existing software or visually interpreted from orthophotos. The evaluation was based on the omission errors, commission errors, and correctness. An omission error refers to a classification failure. Commission errors are caused by misclassification such as when a point belongs to class 'A' but is misclassified as class 'B'. The correctness is the percentage of correct detections.

Correctness rate = True points / Test outcome × 100% (1)
Commission error rate = Commission / Test outcome × 100% (2)
Omission error rate = Omission / Reference data × 100% (3)

Where 'Test outcome' is the classification result, 'True points' is the difference between the reference data and the omission or between the test outcome and the commission.

The bias between the resulting model and the input data is estimated using the root-mean-square error (RMSE):

$$\mathrm{RMSE} = \sqrt{\frac{\sum_{t=1}^{n}(y_t - y)^2}{n}} \quad (4)$$

In **IV**, the RMSE was employed in the evaluation of the results.

4. EXPERIMENTAL RESULTS

4.1 Object detection

Method development

In this thesis, a georeferenced binary image technique was developed for various point cloud classification applications such as building and power line applications. The developed methods typically include the following four steps:

i) 3D point cloud preprocessing or candidate selection;

The criteria for the candidate selection generally include the following: a height threshold, density threshold, and/or histogram threshold. The preprocessing was different for different object detection methods. For example, for building roof detection from ALS, the data were separated into two groups according to the height threshold. One group had points that were 2.5 m above the ground, and the other group included the remaining points.

ii) Transform the candidates into a georeferenced-binary-image;

When a point cloud is transformed into a binary image, the height information is omitted. It is important to choose a proper image pixel size when transforming a 3D point cloud into a binary image. The selection of an image pixel size is affected by the density of the point cloud, particularly for ALS processing.

iii) Image noise removal by applying the parameter thresholds;

The parameters in a binary image typically include the following: the area of an image region, the minor length or/and major length of an image region, and the ratio of the area to the perimeter (the shape of an image region). The proper threshold is applied to filter out the noise. For example, an image region should be line-shaped and narrow for power line detection and rectangular (between a line and circle) when building roofs are detected.

iv) Transform the noise-filtered image back into 3D point cloud.

This step is the inverse of (i). When the binary image is transformed back into a 3D point cloud, the same parameters as those when the point cloud transforms into the binary image should be applied.

The above approach has been applied for building roof detection from ALS, building wall detection from MLS and power line extraction from dense ALS. Figure 1 illustrates the procedure for building roof extraction from ALS point clouds. In **II**, more detailed information was introduced. Figure 2 shows the building wall extraction process using MLS point clouds. A detailed explanation can be found in **I**. The power line extraction from ALS point clouds in a forested area was addressed in **V**. Figure 3 shows the process.

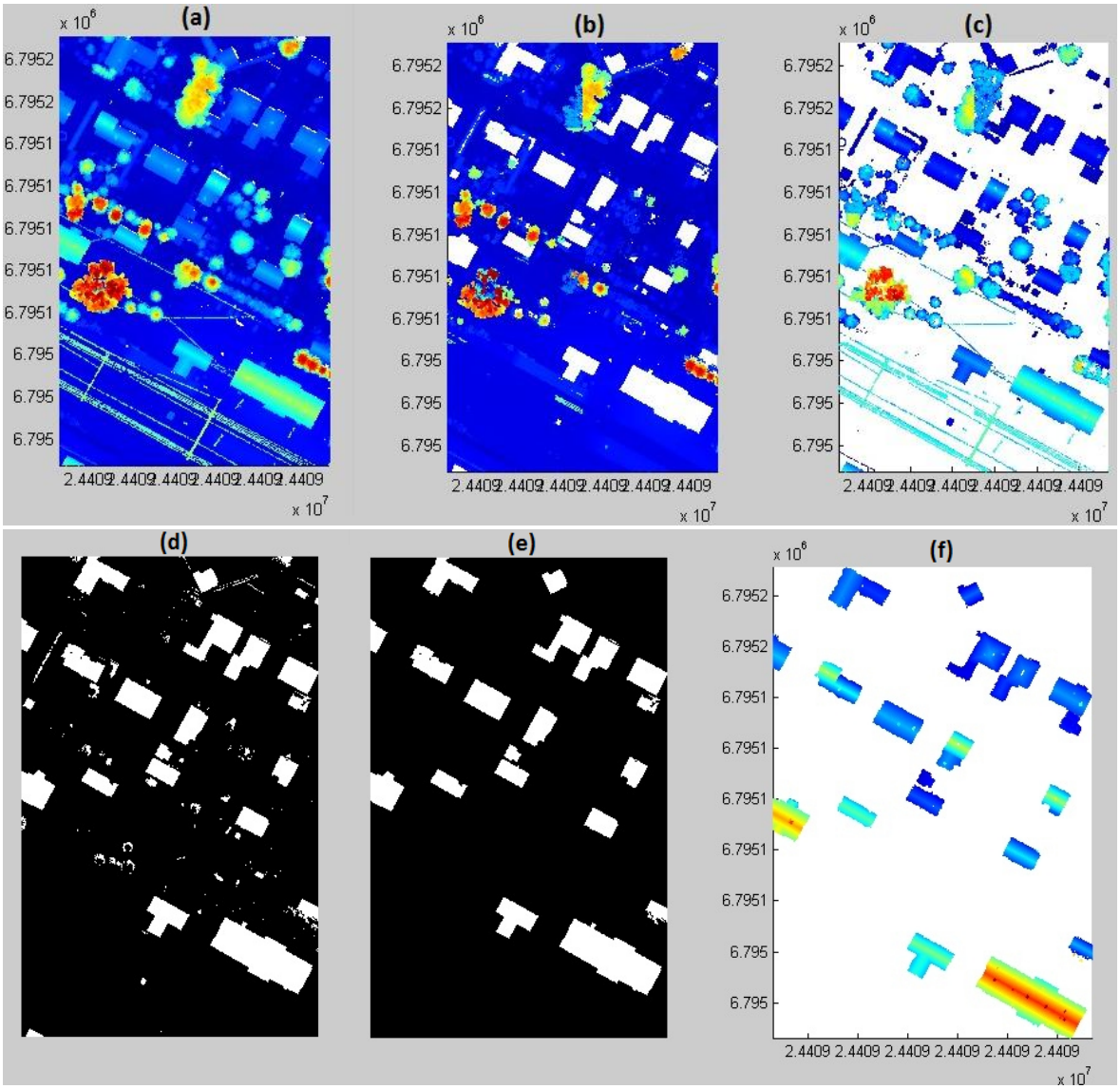

Figure 1. Building extraction from the ALS point cloud. (a) ALS point cloud; (b) Data with height differences from the lowest points of the grid to less than or equal to 2.5 m; (c) Data with height differences from the lowest points of the grid to greater than 2.5 m; (d) A georeferenced binary image from the complementary of (b): Empty is 1; ~empty is 0; (e) Binary image after noise removal; (f) 3D building points. Figure obtained from **II**.

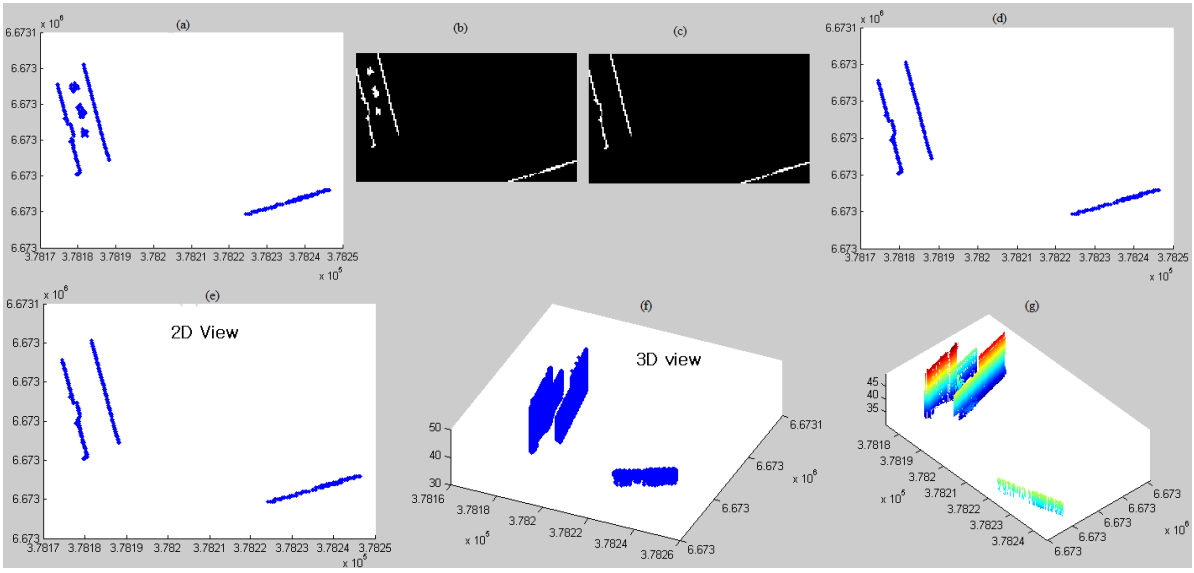

Figure 2. Building wall extraction using an MLS point cloud.
(a) Mobile laser point cloud; (b) A georeferenced-binary-image of (a); (c) Non-building-walls removal from (b); (d) 3D building wall points transformed from a 2D image (c); (e) 2D view from the 3D points (the same as (d)); (f) 3D view of the 3D points; (g) 3D view of the walls with the colors defined by the heights.

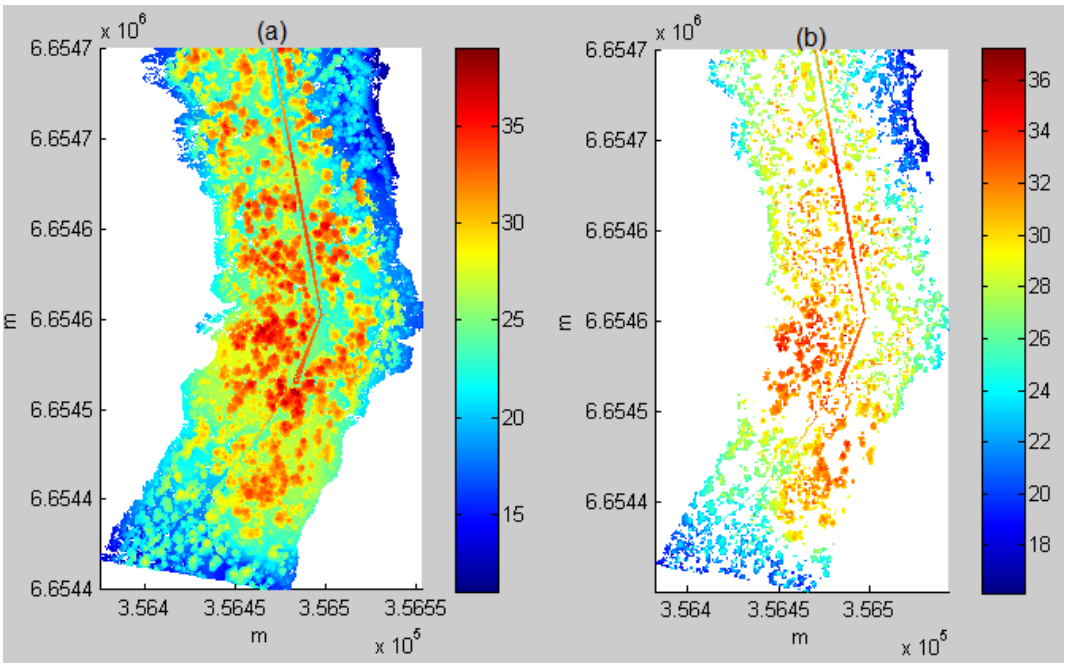

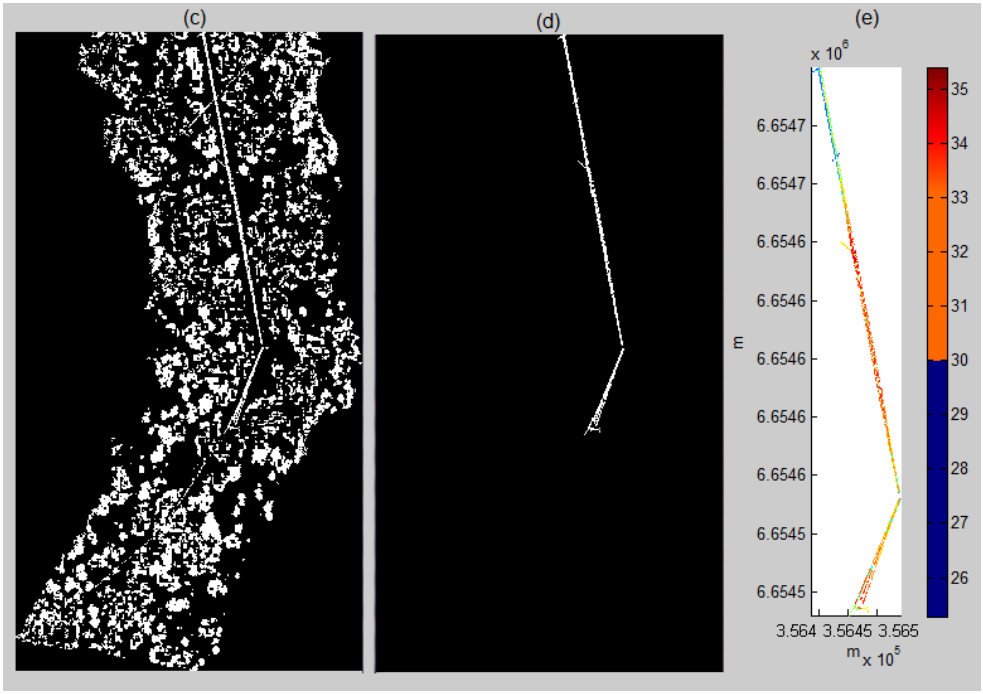

Figure 3. Power line extraction from a dense ALS point cloud in a forested area. (a) ALS point cloud (3D); (b) power line candidate selection (3D); (c) a georeferenced binary image of (b) (2D); (d) after binary image filtering: power line image (2D); (e) extracted power lines (3D). Figure obtained from **V**.

Test results

The detailed results of the object detection process can be found in **I**, **II**, and **V**. Figure 4 shows the results for the building wall extraction using MLS. The test field was located in downtown Tapiola, Espoo, Finland. The data were collected by the FGI ROAMER system. The resulting building facades were used for ground-based building model reconstruction. The 3D building model reconstruction process was semi-automatically performed. Accuracy was assured by interactive visual operation.

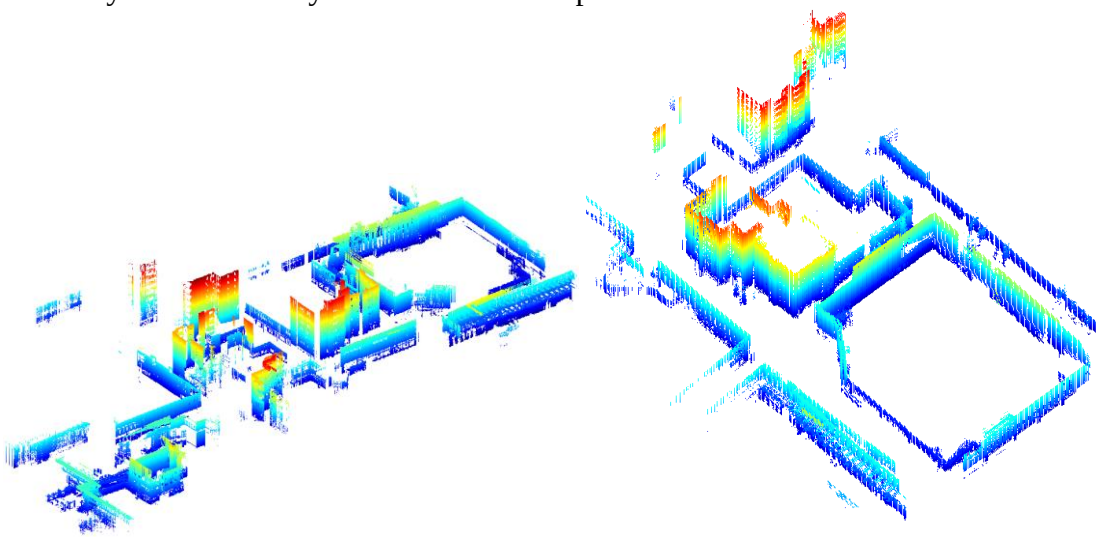

Figure 4. Building wall extraction from a MLS point cloud. (Figure obtained from **I**)

In **II**, the results of the building roof extraction process from ALS were presented. The test field was in Kokemäki, Finland. The ALS data were presented using a density of 50 points/m^2. Figure 5 shows the results. The assessment was performed by comparing the results to an orthophoto with a ground resolution of 20 cm. A total of 57 out of 61 buildings were correctly detected. There were four buildings missing from the results due to their small sizes. In our experiments, a small building was defined as having an area of under 30 m^2.

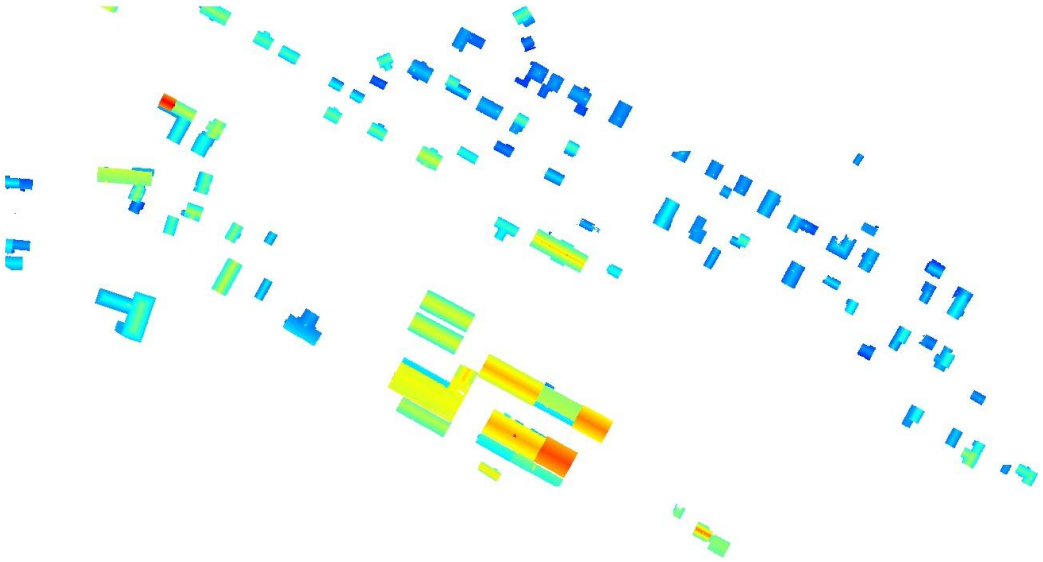

Figure 5. Building roof extraction from an ALS point cloud. (Figure obtained from **IV**)

In **V**, six sets of ALS data from the Kirkkonummi forest areas were utilized to test the power line detection algorithm. The density of the ALS was 50 points/m^2. Figure 6 shows some of the results from the test areas. The lengths of the detected power lines in each area vary between 166 and 464 m. The total length of the power lines is 1.77 km. The reference data included six sets of power line point clouds that were manually and interactively acquired using the Terrascan software package (Terrasolid, Finland). The results were evaluated by statistically evaluating the commission error rate and omission error rate as well as the correctness of the classification. The evaluation reveals that the correctness for different test fields varies from 91.83 to 94.69%. An average correctness of 93.26% was achieved.

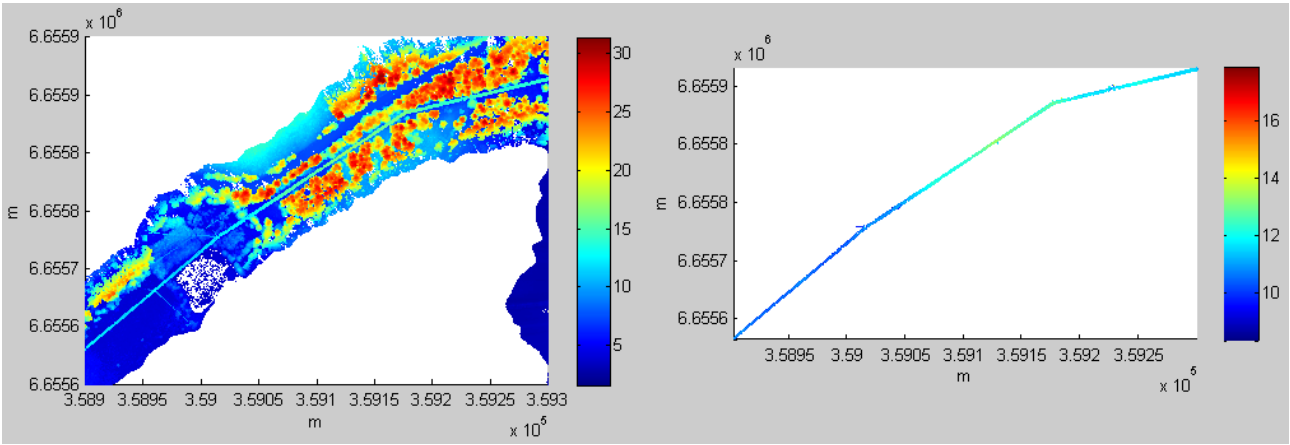

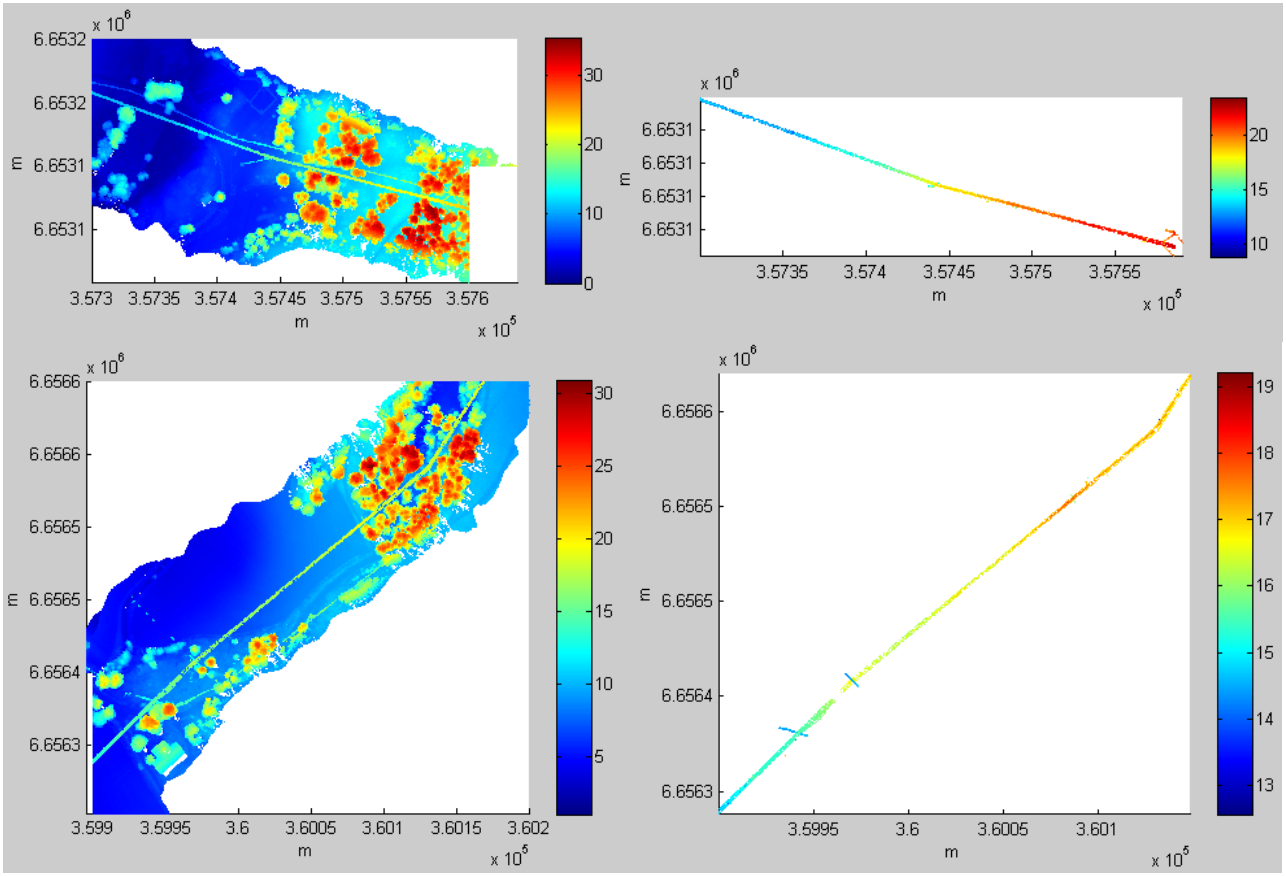

Figure 6. Results of power line extraction from ALS point clouds. Left: ALS point cloud. Right: Extracted power lines. The colors represent the height changes. (Images obtained from **V**)

4.2 Terrain model from ALS

Method development

A terrain model from all ALS points exhibited fairly low efficiency and high computational costs during data post-processing, e.g., surface meshing and model rendering. Whether the terrain is flat or undulated, raster DEMs provide the points with uniform spaces, which produces redundant points for flat terrain and inadequate representation in a changing or sloped area. To overcome this drawback, a quad-tree algorithm was developed to simplify the terrain model.

The quad-tree algorithm is a tree structure that recursively decomposes a square or rectangle into four quadrants, regions, sub-quadrants, and sub-regions (see Figure 7). First, the ALS ground points were divided into four quadrants. The height differences of the ALS points in each quadrant were estimated. If the height difference in the quadrant was greater than a threshold (e.g., 0.3 m), the quadrant was divided into sub-regions, and so on. This process continued until the height differences in all sub-regions were less than the threshold. Thus, the corners of each sub-region were extracted as the model key points. Thus, the number of ground points was greatly reduced.

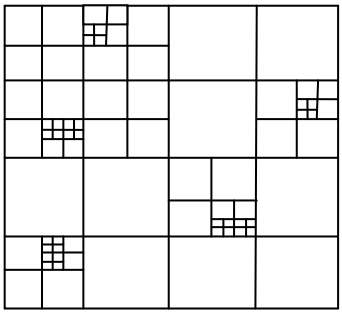

Figure 7. Quadtree algorithm. (Image obtained from **II)**

Test results

In **II**, the results for the terrain model simplification were presented. The test field for the terrain model was located in Kokemäki, Finland. The number of original ALS points was 6,890,129. When the different criteria of the sub-quadrants were applied, the levels of detail of the models were different. In the first image of Figure 8, 113,165 points were presented in the terrain, which is a reduction of 99.36% from the original points. In the second image, the terrain was represented by 181,232 points. The second image experienced a reduction of 97.37% points compared to the original image. The smallest image of Figure 8 represented a well-defined ground surface. There were 252,339 points in the model, representing a 96.34% reduction in the number of points.

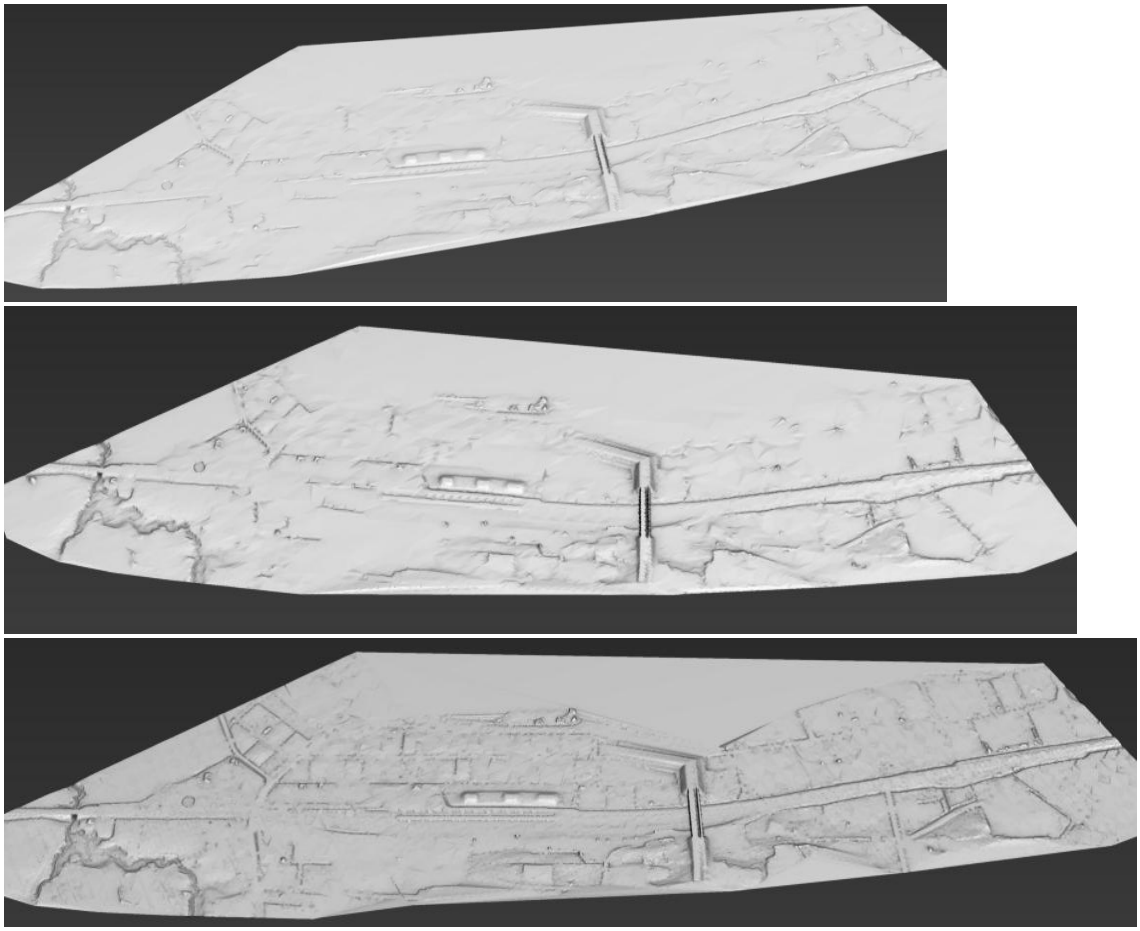

Figure 8. Results of the ground model simplification. The criteria of the sub-quadrants or sub-regions included three levels of detail (LoD): 0.005, 0.01 and 0.02. (Figure obtained from **II**)

4.3 3D road models from open geospatial datasets: ALS and a topographic database

Method development

The approaches for road edge detection and reconstruction were developed based on ALS point clouds and 2D central lines of carriageways from topographic databases. The heights of the central lines of the carriageways could be obtained from ALS data. The approach for road edge acquisition relied on the density of the ALS point cloud. The investigation revealed that the edges of the roads could not be easily defined when the density of the ALS was low. In the case of sparse ALS data, information in topographic databases could be utilized for rough road width estimations; for example, a road with a 'class' of 12111, the width is 10-11 m. If dense ALS data were available, a 'constraint search method' (CSM) was used for the road edge extraction. The CSM approach for road edge detection was developed based on an ALS with a density of 8 points/m^2. The procedure is as follows: i) obtain the elevations of the central lines of carriageways from ALS ground points; ii) determine the ALS search area for the road edge detection; iii) perform road patch separation; iv) use the discrete Laplacian method for road edge detection; v) calculate the width of the road and construct the road's parallel lines on both sides of the central lines according to the detected road width; and vi) triangulate the road edge nodes to form the 3D road network. More detailed information can be found in **IV**.

Test results

In **IV**, a 6*6 km area of a 3D road network was reconstructed. The test data were open geospatial datasets from a Finnish NLS. The data include an ALS point cloud and topographic dataset. The result is shown in Figure 9. Eight roads are selected for the assessments. The assessment was performed by comparing the bias between the detected road widths and the interactive measured widths from the dense ALS points. In addition to the evaluation of the road width bias, the height bias between the ALS points and 3D road models are also included in the assessment process. An average width deviation of 0.22 m and an average height bias of 14cm were achieved.

Figure 9. 3D road network reconstruction from ALS and a topographic database. Upper: an area of 1.5 *1.5 km; Lower: an area of 6 *6 km. (Figure partly obtained from **IV**)

4.4 3D building geometry models from MLS and ALS

In **II**, a railway station in Kokemäki was modeled using ALS data at a density of 50 points/m^2 . A StreetMapper was mounted on a wagon trailer and used to collect the MLS data. The total RMS of ALS was 0.034 m, the average correction of the MLS to match the control points in X, Y, Z directions was less than 10 cm, and the maximum correction was up to 0.4 m. Building modeling as a component in railway environment modeling is demonstrated in Figure 10. The building roofs were constructed with ALS data, whereas the building walls were constructed with MLS data. A randomized Hough transformation method was applied during planar detection. The planar detection equation R = XN*x* + YN*y* +ZNz was used, where X, Y, Z are the coordinates of a point; Nx, Ny, and Nz are the components of the normal vector of a potential plane; and R is the distance between a plane to the origin of the coordinate system. It is critical to select proper thresholds of the parameters to achieve a good result.

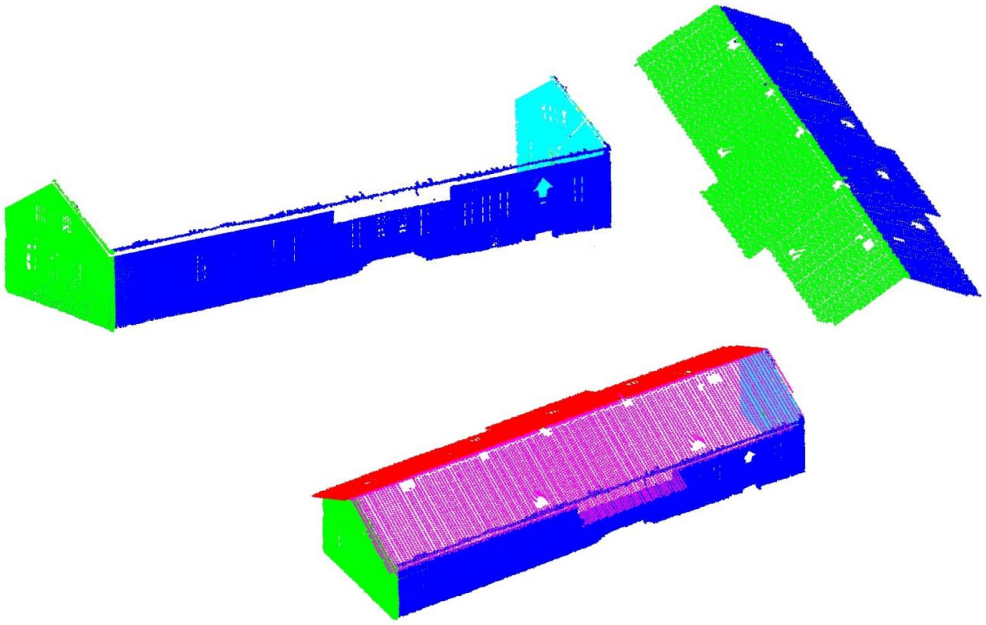

Figure 10. Building obtained from combining the building walls from MLS and the building roofs from ALS. The different colors show the different building planes. Images obtained from **II**.

4.5 3D building geometry models from MLS and UAV images

The MLS data and UAV data had complementary characteristics. The MLS presented detailed data from a ground view. The MLS thus produced an incomplete scene data (e.g. missing data from a top view). The UAV had a low-altitude flight, i.e., at an altitude of 120 m, and a global scene from a top view and oblique view was captured. More detailed information can be found in **III**. The test area was located in Sundsberg, Kirkkonummi, Finland. This area is a residential area with stylish buildings. The MLS data were acquired by the FGI Sensei. The UAV images were obtained from an FGI camera-based UAV. The UAV images were registered by using the poles as control points from the MLS point clouds. Matching the two datasets with an average accuracy of 21.7 cm was achieved. The building facades from the MLS data and roofs from the UAV images were fused to obtain the complete building models. Figure 11 shows the building geometry reconstructed using the MLS and UAV images.

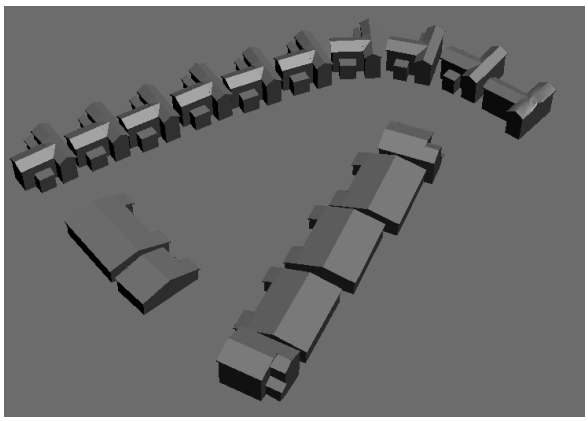

Figure 11. Building geometry reconstruction using MLS and UAV images. Figure obtained from **III**.

4.6 3D building geometry models from ALS

Method development

Automated building reconstruction from the classified ALS building points can be found in **IV**. The proposed approach attempts to solve a problem that is addressed in the literature. Elberink (2010) employed building vectors and an ALS point cloud with a density of 20 points/m^2 for building reconstruction. The author detected the intersection lines and combined them with a ground plan to obtain the building models. The author noted that reconstruction was not feasible when buildings contain complex height jumps and flat roofs because the proposed algorithm could not reliably locate all edges of flat roof segments and because the locations of corner points inside the polygon were not detected. The following procedure was developed to obtain the outlines of the roof segments and reconstruct the buildings with complex height jumps and flat roofs: i) building roof plane detection; ii) building plane data structure establishment; iii) plane outline extraction; iv) step edge recognition and adjustment; v) building ground height acquisition; and vi) building plane meshing.

Roof plane detection and outline extraction are the most critical steps during the reconstruction procedure. Different plane detection approaches were addressed in **I**, **II** and **IV**. In **I**, coplanar points were detected according to the coplanar equation. An initial plane started with random three points, and a fourth point was added to the plane if it satisfied the coplanar equation. This process continued until all points were estimated. In **II**, a plane detection method based on a randomized 3D Hough transformation (RHT) was presented. This approach was based on the normal of the plane. Points with similar normals were selected as coplanar points. An accumulator was established to record the votes from each point. The threshold of the accumulator was critical in determining a plane. In **IV**, a plane detection method was developed based on the seed plane points. First, according to the neighborhoods of the points, the points were divided into planar points and non-planar points. Then, from planar points, a planar seed surface patch was obtained by growing the plane surface. A comparison of the proposed plane detection approaches must be conducted in future work.

Another important step was the plane outline extraction. Building outlines cannot be easily detected in sparse ALS data due to jagged edges in laser point clouds. A method was proposed based on the processing of a georeferenced binary image of the building plane points. First, the plane was rotated so that the area of its minimum boundary box (MBB) was the smallest. Next, the rotated plane (xy plane) was projected to a plane to form a

binary image. Then, the MBB of the image was obtained. Finally, the MBB of its complementary image was acquired. This procedure continued until the solidity of an image was greater than a threshold (e.g., 0.95). The proposed method could be used for both right-angle buildings and non-right-angle buildings. In **IV**, an example for building plane outline extraction from right-angle buildings was introduced (see Figure 12). A detailed procedure is illustrated in Figure 5 to demonstrate the outline extraction for non-right-angle buildings.

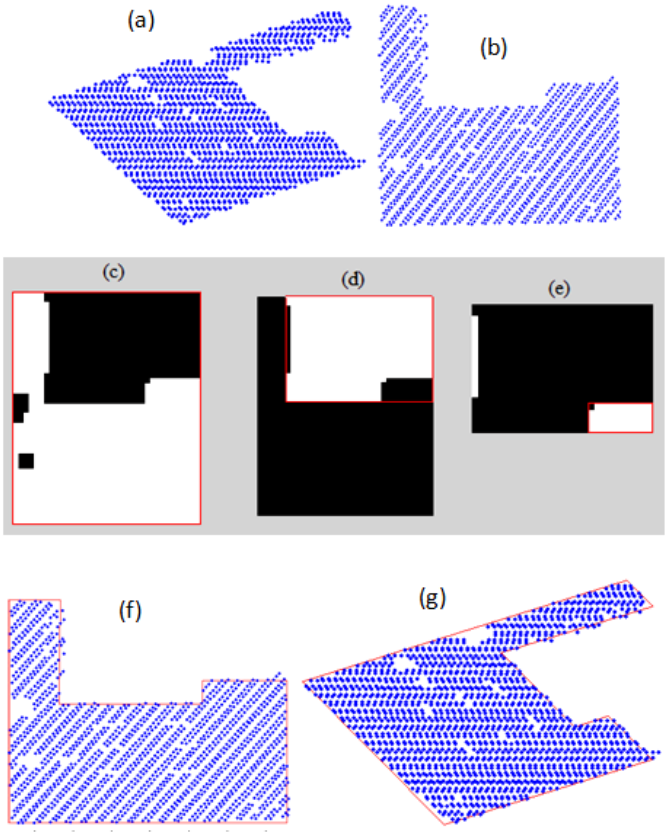

Figure 12. Outline extraction from binary images. (a) Plane point cloud; (b) Plane rotation to the horizontal or vertical direction; (c) Extract the MBB of the plane; (d) Obtain the MBB of the complementary image of (c); (e) Acquire the MBB of the complementary image of (d); (f) Combine the boundaries of (c), (d) and (e) to extract the outline of the plane; (e) Obtain the final outline by rotating the outline of (f) back to the original direction. Figure obtained from **IV**.

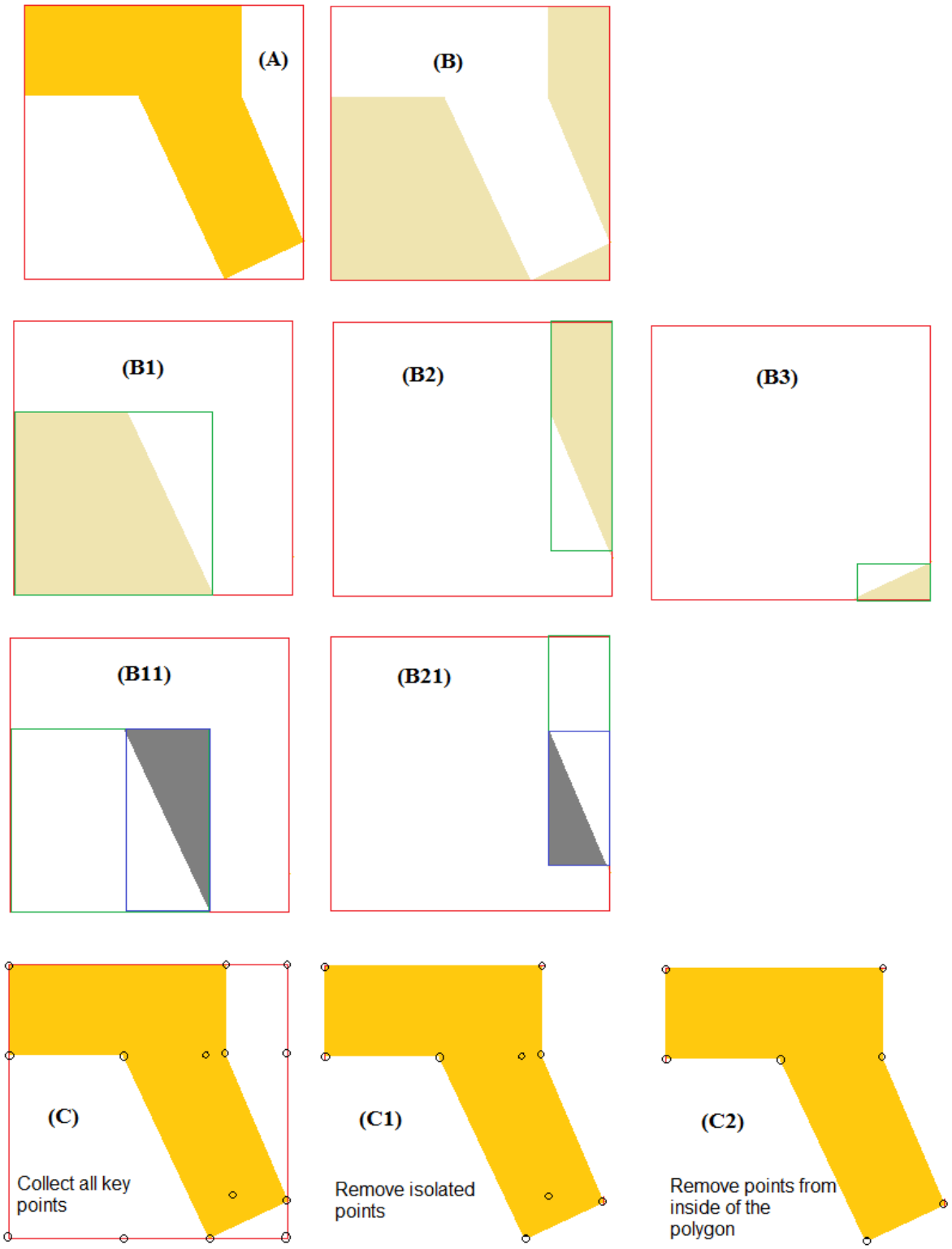

Figure 13. An example of the extraction of the outline of an irregular building roof shape. All images are presented as binary images (object=1 and background =0). Different colors in the figure represent different image regions. (A) An irregular roof represented in yellow; (B) The complementary area of (A); (B1), (B2) and (B3) The sub-regions of (B); (B11) The complementary image of (B1); (B21) The complementary image of (B2); (C) Key points collected from (B11), (B21) and (B3); (C1) Isolated points removed from (C); (C2) Removed points from inside the polygon in (C1).

Figure 14 shows an example of a building geometry reconstructed from an ALS point cloud. Figure 14(a) illustrates ALS building points consisting of multiple planes shown in different colors. The extracted outlines of the planes are shown in Figure 14(b). The following is the step-edge recognition and adjustment. A step-edge is a common edge between two neighboring and height-jumping planes. After plane outline extraction, step edges were identified and adjusted for consistency (see Figure 14(c)). The building base heights could be obtained by projecting the building key points onto a triangulated network of ALS points. After meshing the upper layer of the building points with the base points, building models were generated (see Figure 14 (d)).

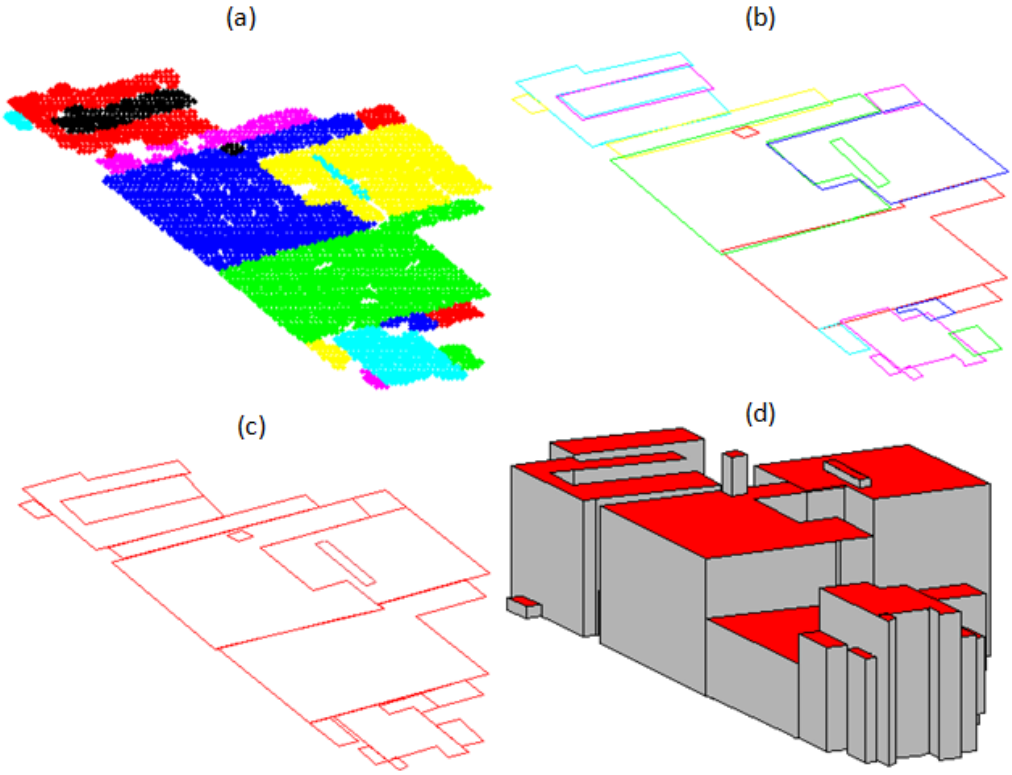

Figure 14. Procedure of building geometry reconstruction. (a) ALS point cloud; (b) Plane outline extraction; (c) Step-edge adjustment; (d) Building geometry reconstruction. In (a) and (b), different colors represent different planes. In (d), gray denotes the building facades, whereas the roofs are filled in red. Figure obtained from **IV**.

Test results

In **IV**, the results for building geometry model acquisition from ALS data were presented. The test field was located in Tapiola, Espoo, Finland. In the test area, most of the buildings included height-jumping flat roofs. A set of ALS point clouds with a density of 0.8 points/m^2 was used. The left image of Figure 15 shows the detected building planes. The right image shows the reconstructed buildings. The results were evaluated in three aspects: i) Evaluation of roof patch detection. The evaluated point cloud contained 236 planar roof patches, and the algorithm detected 271 patches. A total of 176 patches, that is, 74.6% of the building patches, were correctly detected. ii) Evaluation of the distance between the model points and their nearest points in laser data. In our test data, there were 176 roof patches reconstructed, including 1142 model key points extracted. These model key points were compared to their nearest laser points, and the distances were subsequently

calculated. The results showed that 6% of the distances were more than one pixel in size (e.g. 1.6 m in the test data), while 2.5 % of the distances were more than two pixels in size. The pixel size used in the model reconstruction was determined based on the spacing between the input points. Therefore, if a high laser point density is used, the deviation between a model point and its nearest laser point will be reduced. iii) The height difference between the models and the original building points. We selected an even distribution of 15 test locations in the test area, in which we measured the height of both 3D building models and the original building point cloud. We compared the heights of the models and the original points in the locations and estimated the average accuracy of the building models with respect to the original building points. The average height difference between the models and the original points was 15 cm.

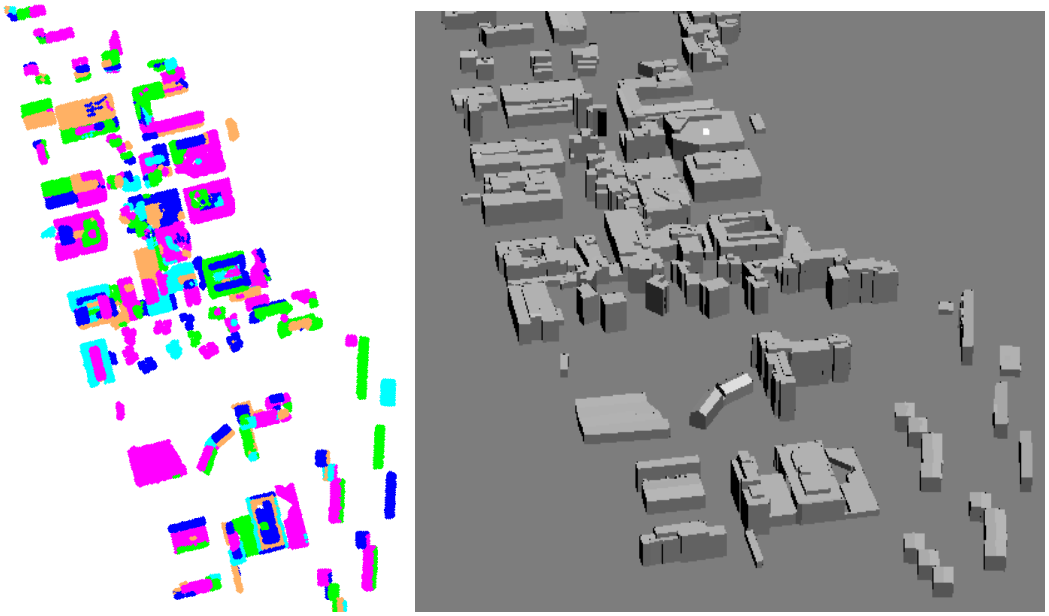

Figure 15. Results of building reconstruction. Left: detected building plane; right: building models. Figure obtained from **IV**.

4.7 Photorealistic 3D building models from MLS

The building models include building geometry models and textures. In this study, the test field was located in downtown Tapiola, Espoo, Finland. This area is an area with commercial buildings, including shopping centers, banks, government agencies, bookstores, and high-rise residential buildings, with the tallest building being 45 m high. Due to the narrow streets in this area, a FGI ROAMER mounted on a trolley was used for data acquisition. The MLS system was accessible for all sides of the buildings. This study indicated that the building models could be reconstructed when the building roofs were flat and the building data were complete.

Models with textures not only offer rich content to guide people's lives, e.g., in personal navigation, but also provide pleasant visualizations. Images are needed for photorealistic building models. The difference between the images and textures lies in the textures being images in which the distortions are corrected. The image distortions include camera lens distortion and perspective distortion. Orthophotos were typically utilized for building roof textures, whereas oblique aerial or terrestrial images were applied for building facades. In this study, terrestrial images were taken separately using a Canon EOS 400D digital camera. Textures were prepared by image distortion correction, and noise was removed from the walls. The resulting models are shown in Figure 16. The models were interactively constructed to achieve good visual quality.

Figure 16. Photorealistic building models. Figure partially obtained from **I**.

5. DISCUSSION

5.1 Quality of the results

Section 4 presented the results from the developed methods. The accuracy of the results was statistically evaluated according to the approaches in Section 3.2. The results provided the following information:

- The quality of automated buildings and power lines extracted from ALS (**II**, **V**);
- The performance of terrain model simplification (**II**);
- The applicability of 3D road network reconstruction from the ALS and topographic database (**IV**);
- The applicability of 3D building geometry models from the MLS and UAV images (**III**);
- The quality of 3D building geometry model reconstruction from ALS (**IV**); and
- The applicability of photorealistic building models from MLS (**I**).

The results of the automated building roof detection using ALS were evaluated by comparing the results to an orthophoto with a ground resolution of 20 cm. The evaluation of the result was presented in **II**. A total of 57 out of 61 buildings were correctly detected (93 %). Four buildings were missing from the results due to their small sizes. In our experiments, buildings that were considered small were defined as having an area of under 30 m^2. The building size threshold is relevant to the used point density. When the points are dense, small objects can be imaged in greater details. Rottensteiner et al. (2007) used ALS data with a density of 1 point per m^2 for building detection. The results showed that 95% of all buildings larger than 70 m^2 were correctly detected and that buildings smaller than 30 m^2 could not be detected. Yang et al. (2014) proposed a marked point process for building extraction from ALS data. The performance was evaluated using the ISPRS benchmark datasets and methods. The ISPRS benchmark ALS datasets included five areas with the density variation of 3.6-6.6 points per m^2. Buildings larger than 50 m^2 in the five datasets were detected with a correctness of 96.6, 100, 97.5, 94.6 and 97%, respectively.

The result from our method was promising. All buildings larger than 30 m^2 were correctly detected in a railway environment. In future studies, more test data should be used.

In **V**, six sets of ALS data with a density of 55 points/m^2 from different forest areas were tested using the developed power line extraction method. The lengths of the detected power lines in each area vary between 166 and 464 m. The total length of the power lines is 1.77 km. The reference data included six sets of power line point clouds acquired manually and interactively using the Terrascan software package (Terrasolid, Finland). The results were evaluated by statistically evaluating the commission error rate and omission error rate as well as the correctness of the classification. The evaluation reveals that the correctness for different test fields varies from 91.8 to 94.7%. An average correctness of 93.3% was achieved. The commission error rate in different datasets varied between 5.3-8.2%. The average commission error rate in the six test fields was 6.7%. The average error rate of omission was 2%. The sources of commission error are mainly from small objects or trees that are attached or are very close to power lines. In this case, certain noise points could not be completely removed. Omission error was mainly caused during candidate selection. When the density criteria and histogram analysis were performed, certain threshold values affected the candidate selection. However, the 93.3% accuracy in the forest environment is a promising result. This finding is comparable with the latest results from non-forest areas such as those reported by Cheng et al. (2014) (93.9%) and by Kim and Sohn (2013) (93.8%).

In **II**, the performance of terrain model simplification method was demonstrated. A set of ALS point clouds with an area with a length of 1000 m and a width of 100 m was tested. In Section 4.2, Figure 8 shows different levels of detail of the simplified terrain model. The corresponding parameters for the sub-region were 0.005, 0.01 and 0.02. There were 6,890,129 original point clouds. When the criterion of the sub-quadrants was set to 0.005, the number of points was reduced by 96.34%, which represented a well-defined ground surface. The number of the points presented in the simplified model was 252,339. When the criterion of the sub-quadrants was set to 0.02, the number of simplified model points was 113,165, exhibiting a reduction of 99.36%. The height accuracy of the target models can be determined based on the criterion of the sub-quadrants. The height accuracy of the target models refers to the height difference in a sub-quadrant, which can be leveled. For example, when the height difference in a terrain was 30 m, the height accuracies of the simplified models were 30*0.005=0.15 m, 30*0.01=0.3 m and 30*0.02=0.6 m for the sub-quadrant criteria 0.005, 0.01 and 0.02, respectively. Typically, the approximation error from the terrain simplification process is measured with respect to the distance from the original, with respect to visual similarity, or with respect to inter-point visibility relationships (Lindstrom and Pascucci, 2002). Because the different levels of detail of the terrain are based on an adjustable parameter, a quantitative measure cannot be used to reflect the errors from different levels of detail. Visual similarity with respect to the original level of detail was utilized in our processing. The method of terrain simplification has been applied to an area of 6*6 km, as presented in **IV**. The resulting model showed sufficient details and pleasant visuals.

In **IV**, two sets of ALS point clouds with different densities (0.8 and 8 points/m^2) for 3D road surface reconstruction were investigated. The results showed that when the density of the point cloud was lower, i.e., 0.8 points/m^2, it was difficult to obtain the edges of the roads using our constrained search method. The road edges were successfully obtained from the dense dataset. Here, the road edge was referenced to the edge of the slope changes. The results were evaluated by comparing the bias between the detected road widths and the interactive measured widths from the dense ALS points. In addition to the evaluation of the road width bias, the height bias between the ALS points and the 3D road

models are also included in the assessment process. The RMSEs of the road widths and heights were estimated by applying equation (4). Eight roads were selected for the assessments. The bias of the road widths varied from 0.15-0.34 m. The average width deviation is 0.22 m. Its RMSE was estimated to be 0.23 m. The deviation of the road heights was between 0.08-0.28m. The average height bias was 0.14 m, with an RMSE of 0.16 m. The width errors are caused by a) noise points around the roads, such as low vegetation close to the road edges, which produces larger detected road widths compared with realistic widths, and b) road parallel assumption. We use the average width and create parallel lines from the central lines to obtain the road edges. In practice, the edges including the road shoulders exhibit zigzag edges, which produce an inconsistency between the measured parallel edges and ideal parallel edges. The height errors may be attributed to the variations in the road surface. The road heights are extracted from the ALS data. The nearby points of each road node located in the ALS ground TIN model are included in the height estimation. An average height value of the nearby points is assigned to the height of the road node. The same height value is applied for the corresponding edge nodes. In most cases, road surfaces are not flat, which creates the potential for errors.

In **III**, the applicability of 3D building geometry models using MLS and UAV images was studied. The results were presented based on two aspects: i) The MLS data and UAV data had complementary characteristics. The MLS provided detailed data from a ground view. This resulted in incomplete scene data (e.g., missing data from a top view). The UAV performed low-altitude flight, i.e., at an altitude of 120 m, and thus, a global scene with a top view and oblique view was captured. However, an oblique view would lead to the occurrence of occlusions in building facades. Therefore, the results from our study demonstrated the advantages of using both datasets for a complete 3D scene reconstruction. ii) The registration between UAV images and MLS point clouds produced an average accuracy of 21.7 cm using the test data from the FGI Sensei (MLS) and the FGI camera-based UAV. The registration was performed by selecting certain points from the MLS point cloud as control points in the UAV image block. Studies using both UAV and MLS data are still quite rare. An example of using both MLS and UAV data can be found in Flener et al. (2013), in which a study on river channel mapping using both types of data was discussed. The author used FGI ROAMER and the FGI UAV system in the study. Ground control target points (GCPs) made of 60 × 60 cm squares of plywood with high-contrast paint and a precise center point were located along the river reaches under survey in fairly regular intervals (Flener et al., 2013). The GCPs were measured using an RTK-GNSS. A georeferenced point cloud was produced from UAV images. The study found that the UAV-based methods can deliver data with accuracies of between 10-20 cm. The difference between our studies might be our choice of software: we only used iWitness for data registration, whereas they used iWitness as the initial solution followed by BAE Systems' Socet Set software for precise orientation. After orientation, Autodesk 123D was employed for georeferencing to the GCPs. It is possible that the adjustment function in the different software packages decreased the probability of errors. Lin and West (2014) proposed the use of UAV images and an MMS system for modeling pole-like objects using the same datasets as we used. Therefore, in the future, more studies on the combined use of MLS and UAV data are needed.

In **IV**, the assessment of 3D building geometry reconstruction using ALS was discussed from three aspects: i) Evaluation of roof patch extraction. The evaluated point cloud contained 236 planar roof patches, and the algorithm detected 271 patches. A total of 176 patches, that is, 74.6% of the building patches, were correctly detected. A total of 41 extracted segments consisted of noise segments that contained non-planar objects such as vegetation or parts of one or more roof patches. A total of 15 instances of under-

segmentation and three instances of over-segmentation were detected; all over-segmented patches were divided into two patches. The extracted patches also included 12 parapets on the edges of the roofs; 16 ambiguous segments, which could be classified as the ground or buildings; and five planar patches that were not parts of buildings. ii) The distance between the model points and their nearest points in the laser data. In our test data, there were 176 reconstructed roof patches, including 1142 extracted model key points. These model key points were compared to their nearest laser points, and the distances were calculated. The results showed that 6% of the distances were more than one pixel in size (e.g., 1.6 m in the test data), and 2.5 % of the distances were more than two pixels in size. The pixel size used during model reconstruction was determined by the distance between the input points. Therefore, if high laser point densities are used, the deviation between a model point and its nearest laser point will be decreased. iii) The height difference between the models and the original building points. We selected 15 evenly distributed test locations in the test area, in which we measured the height of both 3D building models and the original building point cloud. We compared the heights of the models and original points in the locations and estimated the average accuracy of the building models with respect to the original building points. Table 3 shows the height differences between the models and original ALS roof points, which vary from 0 to 0.28 m. We employed the RMSE to measure the bias of the heights. The RMSE can be calculated using equation (4) in Section 3.2. The results showed the height deviation with an RMSE of 18 cm. The average height difference between the models and the original points was 15 cm. The heights of the model key points were determined based on their neighboring points. The referenced height of a roof patch was calculated as an average height of the patch points. Elberink and Vosselman (2011) presented a quality assessment approach for reconstructed 3D building models. The authors proposed using residuals between model faces and laser data and the nearest distance between model points and laser data to measure the quality of the reconstructed building models. Rottensteiner et al. (2014) employed several quality metrics for evaluating the building reconstruction results from ISPRS benchmarks: a) completeness, correctness and quality on a per-roof-plane basis; b) completeness, correctness and quality on a per-roof-plane basis for planes larger than 10 m^2; c) over-segmentation, under-segmentation, and both cases; d) the RMSE of the planimetric distances of the reference roof plane boundary points to their nearest neighbors on the corresponding extracted roof plane boundaries; and e) the RMSE of the height difference between reference planes and all corresponding extracted planes. The reference planes were manually acquired from aerial stereo-images. The quality indices (a) (b) and (c) described the quality of the roof plane segmentation, whereas (d) and (e) represented the geometrical accuracy of the roof polygons. Our assessment method was similar to that of Elberink and Vosselman (2011). However, they evaluated the deviation of the model from each roof patch point.

In **I**, the applicability of photorealistic building models from MLS was demonstrated. The use of MLS data alone for model reconstruction was possible only for the flat roofs and MLS-accessible environment. The roof area can be obtained using surrounded vertical walls, usually similar to a polygon from a top view. However, for other roof types, both ground-based data and aerial-based data are necessary to ensure the completeness of the building models. The model accuracy in our test data was assured by interactive checking and editing. The automation level is relatively low.

5.2 Feasibility of an automated pipeline for 3D building and road reconstruction from ALS and topographic databases for practical applications

ALS has been commercially available since 1994. The development of ALS data has occurred over decades. Currently, numerous commercial software packages for ALS point

cloud processing are available. However, software developers are from different fields or disciplines. The knowledge cannot meet the needs of all customers. For example, some software is able to reconstruct building models for visualization, but they do not perform well in other applications, such as entertainment or transportation. In addition, certain software only supports certain object reconstructions; for example, a software package might be able to reconstruct buildings but not automatically produce 3D roads. Our method was capable of reconstructing various road types, including motorways, highways, urban roads, suburban roads, pedestrian and bicycle roads and tracks. Therefore, our system is more flexible.

The method for building reconstruction was originally developed for reconstructing buildings with height-jumping flat roofs. In practice, this method is applicable to all types of buildings. In Section 4.6, Figure 13 demonstrates the feasibility of irregular building outline extraction. Oblique roofs, such as gable roofs, can also be reconstructed by our method. Gable roofs share a common edge between two roof patches. The procedure for the reconstruction of the gable roof type using our developed method is as follows:

The first step is to detect planar patches from ALS building points (Figure 17(a)). Then, one obtains outlines of each patch (Figure 17(b)). Next, one obtains a common edge by projecting shorter edges onto a longer edge. When the lengths of both neighboring edges are similar, one is projected onto the other one to produce a common edge. When edge 'a' is projected onto edge 'b' and the projected points are not consistent with the ends of edge 'b' (Figure 17(c)), and if the difference is below a threshold (e.g., 1 m), the average location between the projected point and the ending point are estimated (Figure 17(d)). Figure 17 (e) is a 3D view of the reconstructed gable roof.

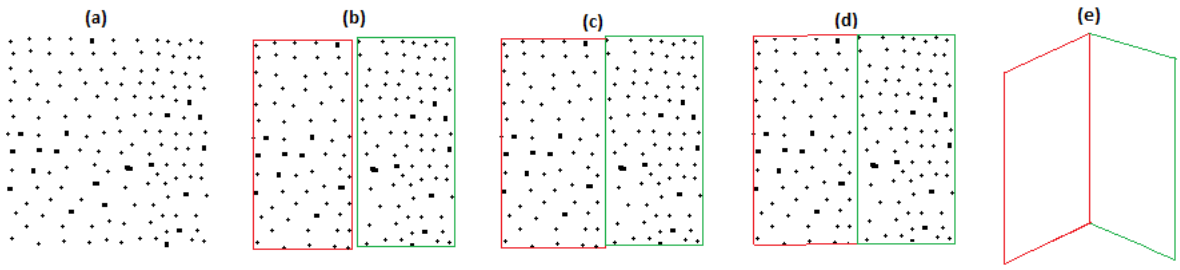

Figure 17. An example of a gable roof reconstructed using our method. (a) Building roof points; (b) Planar patch detection and patch outline extraction; (c) The consistency of the neighboring edges; (d) Neighboring point adjustment; and (e) 3D view of reconstructed gable roof. Figure obtained from **IV**.

The drawback of this method is that it is sensitive to the noise around the edges of the roof patches.

5.3 Feasibility of different levels of detail of building model reconstruction for practical applications

Table 3. Different levels of detail of building models.

LoD of 3D model	Contents	Visualization	Applied data
0	Terrain model	Fly-through view	Open data: ALS
1	Rough building roofs + vertical facades	Fly-through view	Open data from NLS: ALS (0.8 points/m^2)
2	Detailed building roofs + simple building facades	Fly-through view	Espoo municipal data: ALS (8 points/m^2)
3	Building roofs + detailed building facades	Fly-through view and walk-through view	ALS + MLS; UAV+MLS
4	Indoor models	Walk-through view	Not included in this thesis

According to the CityGML standards (CityGML website), the levels of detail (LoDs) of the models can be categorized into five groups: 0-4. Table 3 illustrates the LoDs, the visualization levels and applied data. A LoD of 0 can be achieved using satellite images. Basically, such a model is a terrain model. A LoD of 1-2 is defined according to the details in building roofs. A LoD of 2 for building models also requires some building façade information. A LoD of 1-2 for models is suitable for fly-through views, which means that people visualize the models from hundreds meters away. A LoD of 3 for building models is mainly for street views or walk-through view. Both the model's roofs and the facades can be visualized at a close distance. A LoD of 4 represents indoor models. Many details must be provided.

In the study, we used sparse ALS data for LoD 1 building model reconstruction, and we utilized MLS data combined with ALS data for LoD 3 building model reconstruction. In addition, our study revealed the possibility of using MLS and UAV images for LoD 3 building model reconstruction. In practice, the data fusion of ALS and MLS is feasible for complete building model reconstruction. Using MLS alone, only when building roofs are flat and when MLS is accessible to the building surroundings can the building models be reconstructed. When using UAV images and MLS data, the most challenging aspect was the data registration. If the UAV image orientation parameters were not available, manual measurements from images were necessary to obtain a consistent coordinate system with MLS data.

5.4 Feasibility of 2D topographic database updated to 3D topographic database

The topographic database contains not only the terrain but also the traffic route network, buildings and construction, the administrative borders, geographic names, land use data and waterways. At present, these are in the form of 2D data. However, today's world is a 3D-dominated world. Numerous applications, such as design, entertainment, manufacturing, defense, security, healthcare, public safety and defense, construction, and smart cities, are difficult to develop without 3D data. Currently, only a few countries have

launched the process of updating 2D topographic database to 3D. Among these countries, the Netherlands was the pioneer. Every country has different data storage formats. Roads were presented as 2D road edges in the Netherlands, whereas the central lines of the carriageways were used in Finland.

As the ALS data acquisition continues to expand in Finland, it will cover the entirety of Finland by 2019. This will create the potential for Finnish 2D topographic database upgrades to 3D. The proposed method for 3D building and 3D road models has demonstrated its feasibility. The models for an area of 6 * 6 km were successfully reconstructed. The weakness was that the method was developed in Matlab, in which data processing is relatively slow.

5.5 Feasibility of using different data sources for 3D model reconstruction

The data sources used in this study included three sets of MLS data from different systems, three sets of ALS data with different densities, UAV images and a topographic database.

5.5.1 MLS

In the study, datasets from the FGI ROAMER (**I**), the FGI Sensei (**III**) and the StreetMapper (**II**) have been applied. FGI ROAMER was a Faro laser-scanner-based system with a measurement frequency of 244 kHz. FGI Sensei was based on an Ibeo LUX laser scanner with a maximum point acquisition speed of 38,000 points/s. StreetMapper has a scanning speed of 300 kHz per sensor. These MLSs produced data with different densities and accuracies. The advantages of using MLSs are obvious: fast, detailed and accurate data acquisition for corridor mapping, city furniture extraction, forest inventory and complementary data sources for LoD-3 city models. The flexible platforms of MLS provide the ability to acquire high-resolution data from certain difficult areas, such as using trolley for narrow streets, using wagon trailer for railway environments and using boats for coastlines.

However, a common issue in MLS was that the environment for data acquisition must be selected. The following primary issues must be considered:

i) Occlusion. For example, it was difficult to acquire the building façade data when there were many trees in front of the buildings.

ii) Reflection. When the buildings have a large area of glass walls, the acquired data might be incomplete or extremely noisy. When the area is close to water, the reflection from the water might cause a substantial amount of noise.

5.5.2 ALS

The study of the ALS data can be found in **II**, **IV** and **V**. The densities of the ALS point clouds were 0.8, 8 and 50 points/m^2, respectively. Among these datasets, the data at 0.8 points/m^2 were from the open and free dataset from the NLS; the data at 8 points/m^2 were from a local municipality; and the dense data (50 points/m^2) were from companies. The high-density data results in high data acquisition costs. Since May 2012, the Finnish NLS has started to offer free ALS data. Currently, ALS data cover nearly half of Finland. By 2019, ALS data will cover the entirety of Finland. However, the data update process has been problematic for open and free ALS data. One might use data from several years ago.

ALS has been used in many applications. Currently, ALS is the main means for DEM acquisition, and 3D city models with a LoD of 1-2 from ALS have become popular. As the density of the ALS point cloud increases, increasingly greater numbers of objects can be extracted from ALS data, including power lines (**V**) and roads (**IV**). However, due to the geometry (e.g., direction and height) of ALS data acquisition, some objects are not suitable for extraction from ALS, such as building walls and poles.

- UAV images

In recent years, UAV-based applications have been rapidly expanding. In **III**, UAV images were investigated. The results indicated that UAVs could provide data for an area whereby MLS was not accessible, such as certain private yards. In addition, UAVs can offer data from both top views and oblique views. After UAV data are fused with MLS data, a complete 3D scene can be reconstructed.

The application of using UAV images for 3D city model reconstruction emerged several years ago. The advantage was that the automation level was high (according to C3 technology, it was 98% automated). However, reconstructed 3D models were at a LoD of 2. Occlusions were inevitable when data were acquired from top or oblique views. Therefore, ground-based data (e.g., MLS) are needed to achieve a LoD of three for city models.

- Topographic database

In **IV**, a 2D topographic database was applied for 3D road reconstruction. The development was based on an NLS topographic database, in which the roads were presented as the central lines of carriageways. The approach for 3D road reconstruction was applicable and operable. A 6 *6 km area of the road networks was reconstructed by applying our method.

The topographic database includes not only the central lines of carriageways but also building outlines. In practice, building outlines (also called ground plans) combined with ALS data for 3D building models have been widely used. The CityGML was developed based on the building models reconstructed from ALS and ground plan (CityGML website).

Due to the rich information in the topographic database, it is possible to reconstruct a detailed 3D scene using both ALS and the topographic database. The detailed 3D scene may include terrain, buildings, roads, trees, power lines, vegetation areas and water areas. The LoD of the 3D scene depends on the scale of the topographic database. At present, the open database was at a scale of 1:10,000.

5.6 Further research

The study in this thesis included automated object detection and geometry reconstruction. The trend for future 3D model requirements will be of increasingly greater levels of detail and of increasingly more close-range visual applications as well as having abundant semantic information. Further research will aim for high automation in 3D reconstruction for both outdoor and indoor environment reconstruction; in addition, future research will address not only geometry reconstruction but also automated textured models. In summary, there will be three main tasks in further research:5.6.1 Automated texture mapping

Photorealistic models require textures for objects. Manual texture mapping is time consuming. When provided with images with the correct orientation parameters, the corresponding relationship between an image and model can be established. Thus, the image can be correctly projected onto the model.

5.6.2 Automated indoor 3D model reconstruction

In this thesis, indoor modeling was not included. There are urgent needs for indoor modeling, mapping and navigation. Compared to outdoor environments, indoor objects include less vegetation and more plane-type surfaces. Different shape detection methods will become crucial.

5.6.3 Multi-object 3D scene reconstruction including object semantics or attribute information

A real-world scene is complex and includes many objects. Reconstructed 3D objects, such as buildings and roads, are only a portion of the scene. A topographic database contains many objects and a substantial amount of both geometric and semantic information about the objects. Currently, only part of the database has been used. In the future, a reconstructed 3D scene will include all objects presented in the topographic database, such as terrain, buildings, roads, trees, vegetation areas, water areas, power lines and some individual landmarks. Furthermore, the attributes of these objects will be preserved in 3D models for further 3D applications (e.g., requests from the model or model classification according to their attributes).

6. SUMMARY AND CONCLUSIONS

This thesis has presented automated methods for object detection and 3D building and 3D road reconstruction. The study was based on the hypotheses that object classification approaches for ALS could be automated and that 3D models at different levels of detail could be automatically reconstructed from various data sources. Our study has confirmed these hypotheses. The methodologies were developed based on the following datasets: i) MLS data from three different MLS systems (FGI ROAMER, FGI Sensei and StreetMapper); ii) ALS data with different densities (0.8, 8 and 50 points/m^2); iii) UAV images; iv) a topographic database; and v) orthophotos. A summary of the developed methods is as follows:

- A georeferenced binary image technique was developed for various point cloud classification tasks: building walls from MLS, building roofs from ALS and power line detection from ALS.
- Automated building reconstruction from ALS, including different building plane detection methods and building roof segment outline extraction, was developed and tested.
- Road surfaces were automatically detected by the constrained search method (CSM) and reconstructed from topographic database and ALS.
- A ground model simplification method was developed.

Using the above methods, the following results have been obtained:

- Terrain models with various levels of detail have been obtained. The final number of ALS points representing the terrain can be reduced by up to 99.36% of the original number of points.
- 3D road networks with an area of 6*6 km were reconstructed.
- A railway environment in Kokemäki (Finland) was reconstructed from MLS and ALS.
- UAV images were registered to MLS point clouds, and complete building geometry models were obtained.
- Building geometry models with 236 planes in the Tapiola area (Espoo, Finland) were reconstructed from open ALS data.
- Photorealistic building models for downtown Tapiola (Espoo, Finland) were reconstructed from MLS data. Terrestrial images were applied for building textures.

The above results have been evaluated by comparison to reference data. The reference data were acquired by interactive measurement from existing software and from the orthophoto. The results revealed that an accuracy of 93.4% for the building roof extraction from ALS and an accuracy of 93.3% for power lines extracted from ALS were achieved. In addition, the registration between UAV images and MLS point clouds exhibited an average accuracy of 21.7 cm. In 3D building reconstruction, 74.6% of roof planes were detected,

and the resulting building models from ALS had a height deviation of 15 cm. The distance deviations between the model points and their nearest laser points were estimated. The results showed that 6% of the deviation between the model points and their nearest laser data were more than one pixel in size (e.g., 1.6m in the test data), and 2.5% of them were more than two pixels in size. The pixel size used during model reconstruction was determined based on the spacing between the input points. In 3D road reconstruction, the resulting road models had a width accuracy of 22 cm and a height accuracy of 14 cm.

In practical application, the study has demonstrated the feasibilities of i) automatically producing 3D building and 3D road models from ALS and topographic data; ii) reconstructing different levels of detail of building models; iii) partially updating 2D topographic databases to 3D topographic databases; and iv) using different data sources for 3D model reconstruction.

Further study was recommended to address i) automated texture mapping from aerial and terrestrial images; ii) automated indoor 3D model reconstruction; and iii) multi-object 3D scene reconstruction, including object semantic or attribute information.

Based on the study and obtained results, the contributions of this study can be summarized as follows:

- A georeferenced binary image technique was developed for various 3D point cloud classification.
- Robust methods for the pipeline from original point clouds to 3D model reconstruction were developed.
- The reconstruction of LoDs of 1-3 (referenced to CityGML LoD 0-4) for 3D models was demonstrated.
- The use of different data sources for 3D model reconstruction was studied, and the strengths and weaknesses were addressed.

REFERENCES

1. Arefi, H., Hahn, M., 2005. A morphological reconstruction algorithm for separating off-terrain points from terrain points in laser scanning data. *International Archives of Photogrammetry, Remote Sensing and Spatial Information Sciences*, 36(3/W19).
2. Awrangjeb, M., Fraser, C.S., 2014. Automatic Segmentation of Raw LIDAR Data for Extraction of Building Roofs. *Remote Sensing*, 6(5), 3716-3751.
3. Awrangjeb, M., Zhang, C., Fraser, C.S., 2012. Building detection in complex scenes through effective separation of buildings from trees. *Photogrammetric Engineering & Remote Sensing*, 78 (7), 729–745.
4. Axelsson, P., 2000. DEM generation from laser scanner data using TIN models. In D. Fritsch, M. Molenaar (Eds.), *International Archives of the Photogrammetry and Remote Sensing*, Vol. XXXIII, Part B4/1, pp.110-117.
5. Beger, R., Gedrange, C., Hecht, R., Neubert, M., 2011. Data fusion of extremely high resolution aerial imagery and LIDAR data for automated railroad center line reconstruction. *ISPRS Journal of Photogrammetry and Remote Sensing*, 66, S40–S51.
6. Belgiu, M., Tomljenovic, I., Lampoltshammer, T.J., Blaschke, T., Höfle, B., 2014. Ontology-Based Classification of Building Types Detected from Airborne Laser Scanning Data. *Remote Sensing*, 6(2), 1347-1366.
7. Ben-Moshe, B., Mitchell, J. S., Katz, M. J., Nir, Y., 2002. Visibility preserving terrain simplification: an experimental study. In Proceedings of the eighteenth annual symposium on Computational geometry, pp. 303-311. ACM.
8. Boyko, A., Funkhouser, T., 2011. Extracting roads from dense point clouds in large scale urban environment. *ISPRS Journal of Photogrammetry and Remote Sensing*, 66, S2-S12.
9. Brenner, C., 2000. Towards fully automatic generation of city models. In I. Dowman, & L. Janssen (Eds.). *International Archives of the Photogrammetry and Remote Sensing*: Vol. XXXIII, Part B3, pp. 85-92.
10. Brenner, C., 2004. Modelling 3D objects using weak CSG primitives. International Archives of Photogrammetry, Remote Sensing and Spatial Information Sciences, 35: 1085-1090.
11. Brenner, C., 2005. Building reconstruction from images and laser scanning. *International Journal of Applied Earth Observation and Geoinformation*, 6(3-4), 187-198.
12. Brenner, C., 2009. Extraction of Features from Mobile Laser Scanning Data for Future Driver Assistance systems. In Z. Sester, L. Bernard, & V. Paelke (Eds.), Advances in GIScience, Lecture Notes in Geoinformation and Cartography (pp. 25-42). Springer Verlag.
13. Brenner, C., Haala, N., 1998. Rapid acquisition of virtual reality city models from multiple data sources. In H. Chikatsu & E. Shimizu (Eds.). *The International Archives of the Photogrammetry and Remote Sensing*, Vol. XXXII, Part 5, pp. 323-330.
14. Bulatov, D., Haufel, G., Meidow, J., Pohl, M., Solbrig, P., Wernerus, P., 2014. Context based automatic reconstruction and texturing of 3D urban terrain for quick response tasks. *ISPRS Journal of Photogrammetry and Remote Sensing*, 93, 157– 170.
15. Chen, D., Zhang, L., Li, J., Liu, R., 2012. Urban building roof segmentation from airborne lidar point clouds. *International Journal of Remote Sensing*, 33(20), 6497-6515.
16. Chen, R., Kuusniemi, H., Hyyppä, J., Zhang, J., Takala, J., Kuittinen, R., Chen, Y., Pei, L., Liu, Z., Zhu, L., 2010. Going 3D, Personal Nav and LBS. *GPS World 2010*, 21, 14-18.
17. Chen, R., Pei, Fan, H., Yao, W., Fu, Q., 2014. Segmentation of Sloped Roofs from Airborne LiDAR Point Clouds Using Ridge-Based Hierarchical Decomposition. *Remote Sensing*, 6(4), 3284-3301.

18. CityGML website, 2014. http://www.citygml.org/. Last access, November 20.
19. Clode, S., Rottensteiner, F., 2005. Classification of trees and power lines from medium resolution airborne lasers canner data in urban environments. Proceedings of the APRS Workshop on Digital Image Computing (WDIC), Brisbane, Australia.
20. Clode, S., Rottensteiner, F., Kootsookos, P., Zelniker, E., 2007. Detection and vectorisation of roads from LIDAR data. *Photogrammetric Engineering and Remote Sensing*, 73,517-35.
21. Cornelis, N., Leibe, B., Cornelis, K., Van Gool, L, 2008. 3D urban scene modeling integrating recognition and reconstruction. *International Journal of Computer Vision*, 78, 121-141.
22. Dorninger, P., Pfeifer, N., 2008. A comprehensive automated 3D approach for building extraction, reconstruction, and regularization from airborne laser scanning point clouds. *Sensors*, 8 (11), 7323–7343. doi:10.3390/s8117323.
23. Elberink, S. O., 2008. Problems in automated building reconstruction based on dense airborne laser scanning data. *International Archives of Photogrammetry, Remote Sensing and Spatial Information Sience*, 37, B3.
24. Elberink, S. O., 2010. Acquisition of 3D topography: automated 3D road and building reconstruction using airborne laser scanner data and topographic maps. University of Twente, *PhD Thesis*.
25. Elberink, S. O., Vosselman, G., 2006. Adding the third dimension to a topographic database using airborne laser scanner data. *International Archives of Photogrammetry, Remote Sensing and Spatial Information Sciences*, 36, Part 3, 92-97.
26. Elberink, S. O., Vosselman, G., 2009. Building reconstruction by target based graph matching on incomplete laser data: analysis and limitations. *Sensors*, 9(8), 6101-6118.
27. Elberink, S. O., Vosselman, G., 2011. Quality analysis on 3D building models reconstructed from airborne laser scanning data. *ISPRS Journal of Photogrammetry and Remote Sensing*, 66(2), 157-165.
28. NLS website, 2014. http://www.maanmittauslaitos.fi/. Website last access: 19 August 2014.
29. Fischler, M. A., Bolles, R. C., 1981. Random sample consensus: a paradigm for model fitting with applications to image analysis and automatic cartography. *Communications of the ACM*, 24(6), 381-395.
30. Flener, C., Vaaja, M., Jaakkola, A., Krooks, A., Kaartinen, H., Kukko, A., Alho, P., 2013. Seamless mapping of river channels at high resolution using mobile LiDAR and UAV-photography. *Remote Sensing*, 5(12), 6382-6407.
31. Forlani, G., Nardinocchi, C., Scaioni, M., Zingaretti, P., 2006. Complete classification of raw LIDAR data and 3D reconstruction of buildings. *Pattern Analysis & Applications*, 8(4), 357-374.
32. Fowler, R., Samberg, A., Flood, M., Greaves, T., 2006. Topographic and terrestrial lidar. In D. Maune (Ed.), Digital Elevation Model Technologies & Applications (2nd ed.) (pp. 199- 252).US: Bethesda, Md., *American Society for Photogrammetry and Remote Sensing*.
33. Geospatial world forum, 2014. http://www.geospatialworldforum.org/2012/. Website last access: 19August 2014.
34. Gu, Y., Wu, X., Wang, J., 2014. A Simplification Method of Terrain Modeling Based on Spatial-autocorrelation. *International Journal of Multimedia & Ubiquitous Engineering*, 9(5).
35. Guan, H., Li, J., Yu, Y., Wang, C., Chapman, M., Yang, B., 2014. Using mobile laser scanning data for automated extraction of road markings. ISPRS Journal of Photogrammetry and Remote Sensing, 87, 93-107.

36. Haala, N., Brenner, C., 1999. Virtual City Model from Laser Altimeter and 2D Map Data. Photogrammetric Engineering & Remote Sensing, Vol. 65, no. 7, pp. 787-795.
37. Haala, N., Brenner, C., 1998. Interpretation of Urban Surface Models Using 2D Building Information. *Computer Vision and Image Understanding*, 72, no 2, pp. 204-214.
38. Haala, N., Becker, S., Kada, M., 2006. Cell Decomposition for the Generation of Building Models at Multiple Scales. IAPRS Vol. XXXVI Part III, Symposium Photogrammetric Computer Vision, pp. 19-24.
39. Haala, N., Kada, M., 2004. Generation and application of virtual landscape models for location-based services. Stefanidis, A. & Nittel, S. (eds.) GeoSensor Networks CRC Press.
40. Haala, N., Cramer, M., Rothermel, M., 2013. Quality of 3D Point clouds from highly overlapping UAV Imagery, UAV-g 2013, *International Archives of Photogrammetry, Remote Sensing and Spatial Information Sciences*, XL-1/W2, 183-188, doi:10.5194/isprsarchives-XL-1-W2-183-2013.
41. Haala, N., Kada, M., 2010. An update on automatic 3D building reconstruction. ISPRS J. Photogramm. *Remote Sens*, 65, 570-580.
42. He, Y., Zhang, C., Fraser, C.S., 2014. An energy minimization approach to automated extraction of regular building footprints from airborne LiDAR data. *ISPRS Annals of Photogrammetry, Remote Sensing and Spatial Information Sciences*, 1, 65-72.
43. Hron, V., Halounová, L., 2015. Automatic Generation of 3D Building Models from Point Clouds. In *Geoinformatics for Intelligent Transportation*, pp. 109-119. Springer International Publishing.
44. Huang, H., Brenner, C., Sester, M., 2013. A generative statistical approach to automatic 3D building roof reconstruction from laser scanning data. *ISPRS Journal of Photogrammetry and Remote Sensing*, 79, 29-43.
45. Hyyppä, J., Hyyppä, H., Leckie, D., Gougeon, F., Yu, X., Maltamo, M., 2008. Review of methods of small-footprint airborne laser scanning for extracting forest inventory data in boreal forests. *International Journal of Remote Sensing*, 29(5), 1339-1366.
46. Hyyppä, J., Hyyppä, H., Yu, X., Kaartinen, H., Kukko, A., Holopainen, M., 2009. Forest inventory using small-footprint airborne lidar. In J. Shan, & C. Toth (Eds.): *Topographic Laser Ranging and Scanning: principles and processing*, pp. 335-370. London: CRC Press, Taylor & Fracis.
47. Hyyppä, J., Wagner, W., Hollaus, M., Hyyppä, H., 2009. Airborne Laser Scanning. In T.A. Warner, M.D. Nellis, & G. M. Foody (Eds.): *The SAGE Handbook of remote sensing* (pp. 199-212). London: SAGE Publications.
48. Jaakkola , A., Hyyppä , J., Hyyppä, H., Kukko, A., 2008. Retrieval Algorithms for Road Surface Modeling Using Laser-Based Mobile Mapping. *Sensors*, 8(9), 5238-5249.
49. Jaakkola, A., Hyyppä, J., Kukko, A., Yu, X., Kaartinen, H., Lehtomäki, M., Lin, Y., 2010. A low-cost multi-sensoral mobile mapping system and its feasibility for tree measurements. *ISPRS Journal of Photogrammetry and Remote Sensing*, 65(6), 514–522. doi:10.1016/j.isprsjprs.2010.08.002
50. Jochem, A., Höfle, B., Rutzinger, M., 2011. Extraction of vertical walls from mobile laser scanning data for solar potential assessment. *Remote sensing*, 3(4), 650-667.
51. Jochem, A., Höfle, B., Wichmann, V., Rutzinger, M., Zipf, A., 2012. Area-wide roof plane segmentation in airborne LiDAR point clouds. *Computers, Environment and Urban Systems*, 36(1), 54-64.
52. Jwa, Y., Sohn, G., Kim, H. B., 2009. Automatic 3D Power line reconstruction using airborne Lidar data. Laser scanning, IAPRS, Vol. XXXVIII, Part 3/W8 – Paris, France, September 1-2, 2009.

53. Kaartinen, H., Hyyppä, J., 2006. EuroSDR-Project Commission 3 "Evaluation of Building Extraction", Final Report. (EuroSDR, Official Publication No. 50). MAA: European Spatial Data Research.
54. Karsli, F., Kahya, O., 2012. Detecting the Buildings from Airborne Laser Scanner Data by Using Fourier Transform. *Experimental Techniques*, 36(1), 5-17.
55. Kim, H.B., Sohn, G., 2011. Random forests based multiple classifier system for power-line scene classification. *International Archives of the Photogrammetry, Remote Sensing and Spatial Information Sciences*, Calgary, Canada. Vol. XXXVIII-5/W12, pp. 253-258.
56. Kim, H.B, Sohn, G., 2013. Power-line scene classification with point-based feature from airborne LiDAR data. *Photogrammetric Engineering & Remote Sensing*, 79(9): 821-833.
57. Kim, K., Shan, J., 2011. Building roof modeling from airborne laser scanning data based on level set approach. *ISPRS Journal of Photogrammetry and Remote Sensing*, 66(4), 484-497.
58. Kobler, A.; Pfeifer, N.; Ogrinc, P.; Todorovski, L.; Oštir, K.; Džeroski, S. Repetitive interpolation: a robust algorithm for DTM generation from aerial laser scanner data in forested terrain. *Remote Sens*. Environ. 2007, 108, 9-23.
59. Kraus, K., Pfeifer, N., 1998. Determination of terrain models in wooded areas with airborne laser scanner data. *ISPRS Journal of Photogrammetry and Remote Sensing*, 53, 193–203.
60. Kukko, A., 2009. Road Environment Mapper—3D Data Capturing with Mobile Mapping. Licentiate's Thesis, Helsinki University of Technology, Espoo, Finland, p. 158.
61. Kukko, A., Kaartinen, H., Hyyppa, J., Chen, Y., 2012. Multiplatform mobile laser scanning: Usability and performance. *Sensors*, 12, 11712–11733.
62. Lehtomaki, M., Jaakkola, A., Hyyppa, J., Kukko, A., Kaartinen, H., 2010. Detection of vertical pole-like objects in a road environment using vehicle-based laser scanning data. *Remote Sens.*, 2, 641–664.
63. Liang, Z, Liu, D., Zhou, M., 2014. Research on Large Scale 3D Terrain Generation, Computational Science and Engineering (CSE), 2014 IEEE 17th International Conference on, vol., no., pp.1827, 1832, 19-21 Dec. 2014. doi: 10.1109/CSE.2014.335.
64. Liu, C., Shi, B., Xuan, X., Nan, L., 2012. LEGION segmentation for building extraction from LiDAR data. *International Archives of Photogrammetry, Remote Sensing and Spatial Information Systems*, 39 (Part 3), 291–296.
65. Market research report: 3D modelling and mapping market, 2014. http://www.marketsandmarkets.com/. Website last access: 15 August 2014.
66. Matikainen, L., Hyyppä, J., Hyyppä, H., 2003. Automatic detection of buildings from laser scanner data for map updating. In H.-G. Maas, G. Vosselman, & A. Streilein (Eds.): *The International Archives of Photogrammetry, Remote Sensing and Spatial Information Sciences*, Vol. XXXIV, Part 3/W13 (pp. 218-224).
67. Mayer, H., Hinz, S., Bacher, U., Baltsavias, E., 2006. A test of automatic road extraction approaches. *International Archives of Photogrammetry, Remote Sensing and Spatial Information Systems*, 36 (Part 3), 209–214.
68. McLaughlin, R.A., 2006. Extracting Transmission Lines From Airborne LIDAR Data, *IEEE Geoscience and Remote Sensing Letters*, Vol. 3, NO. 2, pp. 222-226.
69. Melzer, T., 2007. Non-parametric segmentation of ALS point clouds using mean shift. *Journal of Applied Geodesy*, 1(3), 159-170.
70. Melzer, T., Briese, C., 2004. Extraction and modeling of power-lines from ALS point clouds. In Proceedings of 28th Workshop, 47-54.
71. Meng, X., Wang, L., Silván-Cárdenas, J. L., Currit, N., 2009. A multi-directional ground filtering algorithm for airborne LIDAR. *ISPRS Journal of Photogrammetry and Remote Sensing*, 64(1), 117-124.

72. Meng, X., Currit, N., Zhao, K., 2010. Ground filtering algorithms for airborne LiDAR data: a review of critical issues. *Remote Sensing*, 2(3), 833-860.
73. Mongus, D., Lukacˇ, N., Zˇ alik, B., 2014. Ground and building extraction from LiDAR data based on differential morphological profiles and locally fitted surfaces. *ISPRS Journal of Photogrammetry and Remote Sensing*, 93, 145–156.
74. Moussa, A., El-Sheimy, N., 2012. A new object based method for automated extraction of urban objects from airborne sensors data. *International Archives of Photogrammetry, Remote Sensing and Spatial Information Systems*, 39 (Part 3), 309–314.
75. Niemeyer, J., Wegner, J.D., Mallet, C., Rottensteiner, F., Soergel, U., 2011. Conditional random fields for urban scene classification with full waveform LiDAR data. In: Stilla, U., et al. (Eds.), *PIA 2011*, LNCS, vol. 6952, pp. 233–244.
76. Perera, S., Mass, H.-G., 2014. Cycle graph analysis for 3D roof structure modelling: concepts and performance. *ISPRS Journal of Photogrammetry and Remote Sensing*, 93, 213–226.
77. Petrie, G., 2010. An introduction to the technology, mobile mapping systems. *Geoinformatics*, 13, 32-43.
78. Pu, S., Rutzinger, M., Vosselman, G., Elberink, S.O., 2011. Recognizing basic structures from mobile laser scanning data for road inventory studies. *ISPRS Journal of Photogrammetry and Remote Sensing*, 66, 28–39.
79. Rau, J.-Y., Lin, B.-C., 2011. Automatic roof model reconstruction from ALS data and 2D ground plans based on side projection and the TMR algorithm. *ISPRS Journal of Photogrammetry and Remote Sensing*, 66 (6), s13–s27 (supplement).
80. RIEGL Website, 2014. Available online: http://www.riegl.com/ (accessed on 21 January).
81. Rottensteiner, F., Briese, Ch., 2003. Automatic generation of building models from LIDAR data and the integration of aerial images. In: H.-G.Maas, G. Vosselman, & A. Streilein (Eds.), Proceedings of the ISPRS WG III/3 Workshop on ´3-D Reconstruction from Airborne Laserscanner and InSAR data, vol. XXXIV, Part 3/W13 (pp. 174-180). Dresden: IAPRS.
82. Rottensteiner, F., Sohn, G., Gerke, M., Wegner, J.D., Breitkopf, U., Jung, J, 2014. Results of the ISPRS benchmark on urban object detection and 3D building reconstruction. *ISPRS Journal of Photogrammetry and Remote Sensing*, Vol. 93.
83. Rottensteiner, F., Sohn, G., Gerke, M., Wegner, J. D., 2013. ISPRS test project on urban classification and 3D building reconstruction. Commission III-Photogrammetric Computer Vision and Image Analysis, Working Group III/4-3D Scene Analysis, 1-17.
84. Rottensteiner, F., Sohn, G., Jung, J., Gerke, M., Baillard, C., Benitez, S., Breitkopf, U., 2012. The ISPRS benchmark on urban object classification and 3D building reconstruction. *ISPRS Annals of Photogrammetry, Remote Sensing and Spatial Information Sciences*, I-3, 293-298.
85. Rottensteiner, F., Trinder, J., Clode, S., Kubik, K., 2005a. Automated delineation of roof planes from LiDAR data. In G. Vosselman, C. Brenner (Eds.): *The International Archives of the Photogrammetry, Remote Sensing and Spatial Information Sciences*, Vol. XXXVI, Part 3/W4, pp. 221-226.
86. Rottensteiner, F., Trinder, J., Clode, S., Kubik, K., 2005b. Using the Dempster–Shafer method for the fusion of LIDAR data and multispectral images for building detection. *Information Fusion*, 6(4), 283–300.
87. Rutzinger, M., Rottensteiner, F., Pfeifer, N., 2009. A comparison of evaluation techniques for building extraction from airborne laser scanning. *IEEE Journal of Selected Topics in Applied Earth Observations & Remote Sens*., 2 (1), 11–20.

88. Sampath, A., Shan, J., 2010. Segmentation and reconstruction of polyhedral building roofs from aerial LiDAR point clouds. *IEEE Transactions on Geoscience and Remote Sensing*, 48(3), 1554-1567.
89. Seo, S., Lee, J., Kim, Y., 2014. Extraction of Boundaries of Rooftop Fenced Buildings From Airborne Laser Scanning Data Using Rectangle Models. *Geoscience and Remote Sensing Letters*, IEEE 11.2 (2014): 404-408.
90. Sohn, G., Jwa, Y., Kim, H. B., 2012. Automatic power line scene classification and reconstruction using airborne Lidar data. *The International Archives of the Photogrammetry, Remote Sensing and Spatial Information Sciences*, I-3, 167-172, doi:10.5194/isprsannals-I-3-167-2012.
91. Sohn, G., Jwa, Y., Kim, H.B., Jung, J., 2012. An implicit regularization for 3D building rooftop modelling using airborne LiDAR data. *ISPRS Annals of the Photogrammetry, Remote Sensing and Spatial Information Sciences*, 1 (3), 305–310.
92. ShareGeo Open repository, 2014. http://www.sharegeo.ac.uk/. Website last access August 15 2014.
93. Sithole, G., Vosselman, G., 2004. Experimental Comparison of Filter Algorithms for Bare Earth Extraction From Airborne Laser Scanning Point Clouds. *ISPRS Journal of Photogrammetry and Remote Sensing*, 59(1-2), 85-101.
94. Tarsha-kurdi, Fayez, et al., 2007. Model-driven and data-driven approaches using LIDAR data: Analysis and comparison. *International Archives of Photogrammetry, Remote Sensing and Spatial Information Sciences*, 87-92.
95. Toth, C., 2009. R&D of Mobile Mapping and Future Trends. In Proceedings of the ASPRS Annual Conference, Baltimore, MD, USA, 9–13 March.
96. Tournaire, O., Bredif, M., Boldo, D., Durupt, M.. 2010. An efficient stochastic approach for building footprint extraction from digital elevation models. *ISPRS Journal of Photogrammetry and Remote Sensing*, 65(4), 317-327. doi:10.1016/j.isprsjprs.2010.02.002
97. Vögtle, T., Steinle, E., 2003. On the Quality of Object Classification and Automated Building Modeling Based on Laserscanning Data. In H.-G. Maas, G. Vosselman, & A. Streilein (Eds.), *International Archives of Photogrammetry, Remote Sensing and Spatial Information Sciences*, Vol. XXXIV, Part 3/W13 (7p.).
98. Verma, V., Kumar, R., Hsu, S.. 2006. 3D building detection and modeling from aerial LiDAR data. Proceedings of the 2006 IEEE Computer Society Conference on Computer Vision and Pattern Recognition (CVPR'06, 2213-2220.
99. Vosselman, G., 1999. Building Reconstruction Using Planar Faces in Very High Density Height Data. In: *International Archives of Photogrammetry, Remote Sensing and Spatial Information Sciences*, XXXII, part 3/2W5: pp. 87-92.
100. Vosselman, G., Dijkman, S., 2001. 3D building model reconstruction from point clouds and ground plans. *International Archives of the Photogrammetry and Remote Sensing*, Vol. XXXIV, Part 3W4 (pp. 37-43).
101. Vosselman, G., Süveg, I., 2001. Map based building reconstruction from laser data and images. *Automatic Extraction of Man-Made Objects from Aerial and Space Images,* III, pp. 231-239. Ascona, Switzerland: Balkema Publishers.
102. Vosselman, G., 2002. Fusion of laser scanning data, maps, and aerial photographs for building reconstruction. In *IEEE International Geoscience and Remote Sensing Symposium* (IGARSS'02), Vol. 1, pp.85-88.
103. Vosselman, G., 2003. 3D Reconstruction of Roads and Trees for City Modelling. In: *International Archives of Photogrammetry, Remote Sensing and Spatial Information Sciences*, XXXIV, part 3/W13: pp. 231-236.

104. Vosselman, G., B. Gorte, G. Sithole, Rabbani, T., 2004. Recognising Structure in Laser Scanner Point Clouds. In: *International Archives of Photogrammetry, Remote Sensing and Spatial Information Sciences*, XXXVI, part 8 / W2: pp. 33-38.
105. Vosselman, G., Maas, H.-G., 2010. (Eds.). *Airborne and Terrestrial Laser Scanning*. Scotland, Whittles Publising.
106. Wack, R., Wimmer, A., 2002. Digital terrain models from airborne laser scanner data-a grid based approach. *International Archives of Photogrammetry Remote Sensing and Spatial Information Sciences*, 34(3/B), 293-296.
107. Waldhauser, C., Hochreiter, R., Otepka, J., Pfeifer, N., Ghuffar, S., Korzeniowska, K., Wagner, G., 2014. Automated classification of airborne laser scanning point clouds. arXiv preprint arXiv:1404.4304.
108. Xiong, B., Elberink, S. O., Vosselman, G., 2014. A graph edit dictionary for correcting errors in roof topology graphs reconstructed from point clouds. *ISPRS Journal of Photogrammetry and Remote Sensing*, 93, 227–242.
109. Yang, B., Dong, Z., 2013. A shape-based segmentation method for mobile laser scanning point clouds. *ISPRS Journal of Photogrammetry and Remote Sensing*, 81, 19-30.
110. Yang, B., Dong, Z., Zhao, G., Dai, W., 2015. Hierarchical extraction of urban objects from mobile laser scanning data. *ISPRS Journal of Photogrammetry and Remote Sensing*, 99, 45-57.
111. Yang, B., Fang, L., Li, J., 2013. Semi-automated extraction and delineation of 3D roads of street scene from mobile laser scanning point clouds. *ISPRS Journal of Photogrammetry and Remote Sensing*, 79, 80-93.
112. Yang, B., Xu, W., Dong, Z., 2013. Automated building outlines extraction from airborne laser scanning point clouds. *IEEE Geoscience and Remote Sensing Letters*, 5 pages, doi: 10.1109/LGRS.2258887.
113. Yang, B., Xu, W., Yao, W., 2014. Extracting buildings from airborne laser scanning point clouds using a marked point process. *GIScience & Remote Sensing*, 51(5), 555-574.
114. Yan, J., Zhang, K., Zhang, C., Chen, S.C., Narasimhan, G., 2015. Automatic Construction of 3-D Building Model From Airborne LIDAR Data Through 2-D Snake Algorithm. *IEEE Transactions on Geoscience and Remote Sensing*, Volume: 53 Issue 1.
115. Zhang, K., Yan, J., Chen, S., 2006. Automatic construction of building footprints from airborne LIDAR data. *IEEE Transactions on Geoscience and Remote Sensing*, 44(9), 2523-2533.
116. Zhang, W., Grussenmeyer, P., Yan, G., Mohamed, M., 2011. Primitive-based building reconstruction by integration of Lidar data and optical imagery. *International Archives of Photogrammetry, Remote Sensing and Spatial Information Science*, 38, Part 5-W12.
117. Zhao, H., Shibasaki, R., 2003. Reconstructing a textured CAD model of an urban environment using vehicle-borne laser range scanners and line cameras. *Machine Vision and Applications*, 14(1), 35-41.
118. Zhao, H., Shibasaki, R., 2005. Updating digital geographic database using vehicle-borne laser scanners and line cameras. *Photogrammetric Engineering & Remote Sensing*, 71(4), 415-424.

Suomen Geodeettisen laitoksen julkaisut:
Veröffentlichungen des Finnischen Geodätischen Institutes:
Publications of the Finnish Geodetic Institute:

1. Y. VÄISÄLÄ: Tafeln für geodätische Berechnungen nach den Erddimensionen von Hayford. Helsinki 1923. 30 S.
2. Y. VÄISÄLÄ: Die Anwendung der Lichtinterferenz zu Längenmessungen auf grösseren Distanzen. Helsinki 1923. 22 S.
3. ILMARI BONSDORFF, Y. LEINBERG, W. HEISKANEN: Die Beobachtungsergebnisse der südfinnischen Triangulation in den Jahren 1920-1923. Helsinki 1924. 235 S.
4. W. HEISKANEN: Untersuchungen über Schwerkraft und Isostasie. Helsinki 1924. 96 S. 1 Karte.
5. W. HEISKANEN: Schwerkraft und isostatische Kompensation in Norwegen. Helsinki 1926. 33 S. 1 Karte.
6. W. HEISKANEN: Die Erddimensionen nach den europäischen Gradmessungen. Helsinki 1926. 26 S.
7. ILMARI BONSDORFF, V.R. ÖLANDER, Y. LEINBERG: Die Beobachtungsergebnisse der südfinnischen Triangulation in den Jahren 1924-1926. Helsinki 1927. 164 S. 1 Karte.
8. V.R. ÖLANDER: Ausgleichung einer Dreieckskette mit Laplaceschen Punkten. Helsinki 1927. 49 S. 1 Karte.
9. U. PESONEN: Relative Bestimmungen der Schwerkraft auf den Dreieckspunkten der südfinnischen Triangulation in den Jahren 1924-1925. Helsinki 1927. 129 S.
10. ILMARI BONSDORFF: Das Theorem von Clairaut und die Massenverteilung im Erdinnern. Helsinki 1929. 10 S.
11. ILMARI BONSDORFF, V.R. ÖLANDER, W. HEISKANEN, U. PESONEN: Die Beobachtungsergebnisse der Triangulationen in den Jahren 1926-1928. Helsinki 1929. 139 S. 1 Karte.
12. W. HEISKANEN: Über die Elliptizität des Erdäquators. Helsinki 1929. 18 S.
13. U. PESONEN: Relative Bestimmungen der Schwerkraft in Finnland in den Jahren 1926-1929. Helsinki 1930. 168 S. 1 Karte.
14. Y. VÄISÄLÄ: Anwendung der Lichtinterferenz bei Basismessungen. Helsinki 1930. 47 S.
15. M. FRANSSILA: Der Einfluss der den Pendel umgebenden Luft auf die Schwingungszeit beim v. Sterneckschen Pendelapparat. Helsinki 1931. 23 S.
16. Y. LEINBERG: Ergebnisse der astronomischen Ortsbestimmungen auf den finnischen Dreieckspunkten. Helsinki 1931. 162 S.
17. V.R. ÖLANDER: Über die Beziehung zwischen Lotabweichungen und Schwereanomalien sowie über das Lotabweichungssystem in Süd-Finnland. Helsinki 1931. 23 S.
18. PENTTI KALAJA, UUNO PESONEN, V.R. ÖLANDER, Y. LEINBERG: Beobachtungsergebnisse. Helsinki 1933. 240 S. 1 Karte.
19. R.A. HIRVONEN: The continental undulations of the geoid. Helsinki 1934. 89 pages. 1 map.
20. ILMARI BONSDORFF: Die Länge der Versuchsbasis von Helsinki und Längenveränderungen der Invardrähte 634-637. Helsinki 1934. 41 S.
21. V.R. ÖLANDER: Zwei Ausgleichungen des grossen südfinnischen Dreieckskranzes. Helsinki 1935. 66 S. 1 Karte.
22. U. PESONEN, V.R. ÖLANDER: Beobachtungsergebnisse. Winkelmessungen in den Jahren 1932-1935. Helsinki 1936. 148 S. 1 Karte.
23. R.A. HIRVONEN: Relative Bestimmungen der Schwerkraft in Finnland in den Jahren 1931, 1933 und 1935. Helsinki 1937. 151 S.
24. R.A. HIRVONEN: Bestimmung des Schwereunterschiedes Helsinki-Potsdam im Jahre 1935 und Katalog der finnischen Schwerestationen. Helsinki 1937. 36 S. 1 Karte.
25. T.J. KUKKAMÄKI: Über die nivellitische Refraktion. Helsinki 1938. 48 S.
26. Finnisches Geodätisches Institut 1918-1938. Helsinki 1939. 126 S. 2 Karten.
27. T.J. KUKKAMÄKI: Formeln und Tabellen zur Berechnung der nivellitischen Refraktion. Helsinki 1939. 18 S.
28. T.J. KUKKAMÄKI: Verbesserung der horizontalen Winkelmessungen wegen der Seitenrefraktion. Helsinki 1939. 18 S.
29. ILMARI BONSDORFF: Ergebnisse der astronomischen Ortsbestimmungen im Jahre 1933. Helsinki 1939. 47 S.
30. T. HONKASALO: Relative Bestimmungen der Schwerkraft in Finnland im Jahre 1937. Helsinki 1941. 78 S.
31. PENTTI KALAJA: Die Grundlinienmessungen des Geodätischen Institutes in den Jahren 1933-1939 nebst Untersuchungen über die Verwendung der Invardrähte. Helsinki 1942. 149 S.
32. U. PESONEN, V.R. ÖLANDER: Beobachtungsergebnisse. Winkelmessungen in den Jahren 1936-1940. Helsinki 1942. 165 S. 1 Karte.
33. PENTTI KALAJA: Astronomische Ortsbestimmungen in den Jahren 1935-1938. Helsinki 1944. 142 S.
34. V.R. ÖLANDER: Astronomische Azimutbestimmungen auf den Dreieckspunkten in den Jahren 1932-1938; Lotabweichungen und Geoidhöhen. Helsinki 1944. 107 S. 1 Karte.
35. U. PESONEN: Beobachtungsergebnisse. Winkelmessungen in den Jahren 1940-1947. Helsinki 1948. 165 S. 1 Karte.
36. Professori Ilmari Bonsdorffille hänen 70-vuotispäivänään omistettu juhlajulkaisu. Publication dedicated to Ilmari Bonsdorff on the occasion of his 70th anniversary. Helsinki 1949. 262 pages. 13 maps.
37. TAUNO HONKASALO: Measuring of the 864 m-long Nummela standard base line with the Väisälä light interference comparator and some investigations into invar wires. Helsinki 1950. 88 pages.
38. V.R. ÖLANDER: On the geoid in the Baltic area and the orientation of the Baltic Ring. Helsinki 1950. 26 pages.
39. W. HEISKANEN: On the world geodetic system. Helsinki 1951. 25 pages.
40. R.A. HIRVONEN: The motions of Moon and Sun at the solar eclipse of 1947 May 20th. Helsinki 1951. 36 pages.
41. PENTTI KALAJA: Catalogue of star pairs for northern latitudes from 55° to 70°for astronomic determination of latitudes by the Horrebow-Talcott method. Helsinki 1952. 191 pages.
42. ERKKI KÄÄRIÄINEN: On the recent uplift of the Earth's crust in Finland. Helsinki 1953. 106 pages. 1 map.
43. PENTTI KALAJA: Astronomische Ortsbestimmungen in den Jahren 1946-1948. Helsinki 1953. 146 S.
44. T.J. KUKKAMÄKI, R.A. HIRVONEN: The Finnish solar eclipse expeditions to the Gold Coast and Brazil 1947. Helsinki 1954. 71 pages.
45. JORMA KORHONEN: Einige Untersuchungen über die Einwirkung der Abrundungsfehler bei Gross-Ausgleichungen. Neu-Ausgleichung des südfinnischen Dreieckskranzes. Helsinki 1954. 138 S. 3 Karten.

46. Professori Weikko A. Heiskaselle hänen 60-vuotispäivänään omistettu juhlajulkaisu. Publication dedicated to Weikko A. Heiskanen on the occasion of his 60th anniversary. Helsinki 1955. 214 pages.
47. Y. VÄISÄLÄ: Bemerkungen zur Methode der Basismessung mit Hilfe der Lichtinterferenz. Helsinki 1955. 12 S.
48. U. PESONEN, TAUNO HONKASALO: Beobachtungsergebnisse der finnischen Triangulationen in den Jahren 1947-1952. Helsinki 1957. 91 S.
49. PENTTI KALAJA: Die Zeiten von Sonnenschein, Dämmerung und Dunkelheit in verschiedenen Breiten. Helsinki 1958. 63 S.
50. V.R. ÖLANDER: Astronomische Azimutbestimmungen auf den Dreieckspunkten in den Jahren 1938-1952. Helsinki 1958. 90 S. 1 Karte.
51. JORMA KORHONEN, V.R. ÖLANDER, ERKKI HYTÖNEN: The results of the base extension nets of the Finnish primary triangulation. Helsinki 1959. 57 pages. 5 appendices. 1 map.
52. V.R. ÖLANDER: Vergleichende Azimutbeobachtungen mit vier Instrumenten. Helsinki 1960. 48 pages.
53. Y. VÄISÄLÄ, L. OTERMA: Anwendung der astronomischen Triangulationsmethode. Helsinki 1960. 18 S.
54. V.R. ÖLANDER: Astronomical azimuth determinations on trigonometrical stations in the years 1955-1959. Helsinki 1961. 15 pages.
55. TAUNO HONKASALO: Gravity survey of Finland in years 1945-1960. Helsinki 1962. 35 pages. 3 maps.
56. ERKKI HYTÖNEN: Beobachtungsergebnisse der finnischen Triangulationen in den Jahren 1953-1962. Helsinki 1963. 59 S.
57. ERKKI KÄÄRIÄINEN: Suomen toisen tarkkavaaituksen kiintopisteluettelo I. Bench mark list I of the Second Levelling of Finland. Helsinki 1963. 164 pages. 2 maps.
58. ERKKI HYTÖNEN: Beobachtungsergebnisse der finnischen Triangulationen in den Jahren 1961-1962. Helsinki 1963. 32 S.
59. AIMO KIVINIEMI: The first order gravity net of Finland. Helsinki 1964. 45 pages.
60. V.R. ÖLANDER: General list of astronomical azimuths observed in 1920-1959 in the primary triangulation net. Helsinki 1965. 47 pages. 1 map.
61. ERKKI KÄÄRIÄINEN: The second levelling of Finland in 1935-1955. Helsinki 1966. 313 pages. 1 map.
62. JORMA KORHONEN: Horizontal angles in the first order triangulation of Finland in 1920-1962. Helsinki 1966. 112 pages. 1 map.
63. ERKKI HYTÖNEN: Measuring of the refraction in the Second Levelling of Finland. Helsinki 1967. 18 pages.
64. JORMA KORHONEN: Coordinates of the stations in the first order triangulation of Finland. Helsinki 1967. 42 pages. 1 map.
65. Geodeettinen laitos - The Finnish Geodetic Institute 1918-1968. Helsinki 1969. 147 pages. 4 maps.
66. JUHANI KAKKURI: Errors in the reduction of photographic plates for the stellar triangulation. Helsinki 1969. 14 pages.
67. PENTTI KALAJA, V.R. ÖLANDER: Astronomical determinations of latitude and longitude in 1949-1958. Helsinki 1970. 242 pages. 1 map.
68. ERKKI KÄÄRIÄINEN: Astronomical determinations of latitude and longitude in 1954-1960. Helsinki 1970. 95 pages. 1 map.
69. AIMO KIVINIEMI: Niinisalo calibration base line. Helsinki 1970. 36 pages. 1 sketch appendix.
70. TEUVO PARM: Zero-corrections for tellurometers of the Finnish Geodetic Institute. Helsinki 1970. 18 pages.
71. ERKKI KÄÄRIÄINEN: Astronomical determinations of latitude and longitude in 1961-1966. Helsinki 1971. 102 pages. 1 map.
72. JUHANI KAKKURI: Plate reduction for the stellar triangulation. Helsinki 1971. 38 pages.
73. V.R. ÖLANDER: Reduction of astronomical latitudes and longitudes 1922-1948 into FK4 and CIO systems. Helsinki 1972. 40 pages.
74. JUHANI KAKKURI AND KALEVI KALLIOMÄKI: Photoelectric time micrometer. Helsinki 1972. 53 pages.
75. ERKKI HYTÖNEN: Absolute gravity measurement with long wire pendulum. Helsinki 1972. 142 pages.
76. JUHANI KAKKURI: Stellar triangulation with balloon-borne beacons. Helsinki 1973. 48 pages.
77. JUSSI KÄÄRIÄINEN: Beobachtungsergebnisse der finnischen Winkelmessungen in den Jahren 1969-70. Helsinki 1974. 40 S.
78. AIMO KIVINIEMI: High precision measurements for studying the secular variation in gravity in Finland. Helsinki 1974. 64 pages.
79. TEUVO PARM: High precision traverse of Finland. Helsinki 1976. 64 pages.
80. R.A. HIRVONEN: Precise computation of the precession. Helsinki 1976. 25 pages.
81. MATTI OLLIKAINEN: Astronomical determinations of latitude and longitude in 1972-1975. Helsinki 1977. 90 pages. 1 map.
82. JUHANI KAKKURI AND JUSSI KÄÄRIÄINEN: The Second Levelling of Finland for the Aland archipelago. Helsinki 1977. 55 pages.
83. MIKKO TAKALO: Suomen Toisen tarkkavaaituksen kiintopisteluettelo II. Bench mark list II of the Second Levelling of Finland. Helsinki 1977. 150 sivua.
84. MATTI OLLIKAINEN: Astronomical azimuth determinations on triangulation stations in 1962-1970. Helsinki 1977. 47 pages. 1 map.
85. MARKKU HEIKKINEN: On the tide-generating forces. Helsinki 1978. 150 pages.
86. PEKKA LEHMUSKOSKI AND JAAKKO MÄKINEN: Gravity measurements on the ice of Bothnian Bay. Helsinki 1978. 27 pages.
87. T.J. KUKKAMÄKI: Väisälä interference comparator. Helsinki 1978. 49 pages.
88. JUSSI KÄÄRIÄINEN: Observing the Earth Tides with a long water-tube tiltmeter. Helsinki 1979. 74 pages.
89. Publication dedicated to T.J. Kukkamäki on the occasion of his 70th anniversary. Helsinki 1979. 184 pages.
90. B. DUCARME AND J. KÄÄRIÄINEN: The Finnish Tidal Gravity Registrations in Fennoscandia. Helsinki 1980. 43 pages.
91. AIMO KIVINIEMI: Gravity measurements in 1961-1978 and the results of the gravity survey of Finland in 1945-1978. Helsinki 1980. 18 pages. 3 maps.
92. LIISI OTERMA: Programme de latitude du tube zénithal visuel de l'observatoire Turku-Tuorla systéme amélioré de 1976. Helsinki 1981. 18 pages.
93. JUHANI KAKKURI, AIMO KIVINIEMI AND RAIMO KONTTINEN: Contributions from the Finnish Geodetic Institute to the Tectonic Plate Motion Studies in the Area between the Pamirs and Tien-Shan Mountains. Helsinki 1981. 34 pages.
94. JUSSI KÄÄRIÄINEN: Measurement of the Ekeberg baseline with invar wires. Helsinki 1981. 17 pages.
95. MATTI OLLIKAINEN: Astronomical determinations of latitude and longitude in 1976-1980. Helsinki 1982. 90 pages. 1 map.
96. RAIMO KONTTINEN: Observation results. Angle measurements in 1977-1978. Helsinki 1982. 29 pages.

97. G.P. ARNAUTOV, YE N. KALISH, A. KIVINIEMI, YU F. STUS, V.G. TARASIUK, S.N. SCHEGLOV: Determination of absolute gravity values in Finland using laser ballistic gravimeter. Helsinki 1982. 18 pages.
98. LEENA MIKKOLA (EDITOR): Mean height map of Finland. Helsinki 1983. 3 pages. 1 map.
99. MIKKO TAKALO AND JAAKKO MÄKINEN: The Second Levelling of Finland for Lapland. Helsinki 1983. 144 pages.
100. JUSSI KÄÄRIÄINEN: Baseline Measurements with invar wires in Finland 1958-1970. Helsinki 1984. 78 pages.
101. RAIMO KONTTINEN: Plate motion studies in Central Asia. Helsinki 1985. 31 pages.
102. RAIMO KONTTINEN: Observation results. Angle measurements in 1979-1983. Helsinki 1985. 30 pages.
103. J. KAKKURI, T.J. KUKKAMÄKI, J.-J. LEVALLOIS ET H. MORITZ: Le 250^{e} anniversaire de la mesure de l'arc du meridien en Laponie. Helsinki 1986. 60 pages.
104. G. ASCH, T. JAHR, G. JENTZSCH, A. KIVINIEMI AND J. KÄÄRIÄINEN: Measurements of Gravity Tides along the "Blue Road Geotraverse" in Fennoscandia. Helsinki 1987. 57 pages.
105. JUSSI KÄÄRIÄINEN, RAIMO KONTTINEN, LU QIANKUN AND DU ZONG YU: The Chang Yang Standard Baseline. Helsinki 1986. 36 pages.
106. E.W. GRAFAREND, H. KREMERS, J. KAKKURI AND M. VERMEER: Adjusting the SW Finland Triangular Network with the TAGNET 3-D operational geodesy software. Helsinki 1987. 60 pages.
107. MATTI OLLIKAINEN: Astronomical determinations of latitude and longitude in 1981-1983. Helsinki 1988. 37 pages.
108. MARKKU POUTANEN: Observation results. Angle measurements in 1967-1973. Helsinki 1988. 35 pages.
109. JUSSI KÄÄRIÄINEN, RAIMO KONTTINEN AND ZSUZSANNA NÉMETH: The Gödöllö Standard Baseline. Helsinki 1988. 66 pages.
110. JUSSI KÄÄRIÄINEN AND HANNU RUOTSALAINEN: Tilt measurements in the underground laboratory Lohja 2, Finland, in 1977-1987. Helsinki 1989. 37 pages.
111. MIKKO TAKALO: Lisäyksiä ja korjauksia Suomen tarkkavaaitusten linjastoon 1977-1989. Helsinki 1991. 98 sivua.
112. RAIMO KONTTINEN: Observation results. Angle measurements in the Pudasjärvi loop in 1973-1976. Helsinki 1991. 42 pages.
113. RAIMO KONTTINEN, JORMA JOKELA AND LI QUAN: The remeasurement of the Chang Yang Standard Baseline. Helsinki 1991. 40 pages.
114. JUSSI KÄÄRIÄINEN, RAIMO KONTTINEN AND MARKKU POUTANEN: Interference measurements of the Nummela Standard Baseline in 1977, 1983, 1984 and 1991. Helsinki 1992. 78 pages.
115. JUHANI KAKKURI (EDITOR): Geodesy and geophysics. Helsinki 1993. 200 pages.
116. JAAKKO MÄKINEN, HEIKKI VIRTANEN, QIU QI-XIAN AND GU LIANG-RONG: The Sino-Finnish absolute gravity campaign in 1990. Helsinki 1993. 49 pages.
117. RAIMO KONTTINEN: Observation results. Geodimeter observations in 1971-72, 1974-80 and 1984-85. Helsinki 1994. 58 pages.
118. RAIMO KONTTINEN: Observation results. Angle measurements in 1964-65, 1971, 1984 and 1986-87. Helsinki 1994. 67 pages.
119. JORMA JOKELA: The 1993 adjustment of the Finnish First-Order Terrestrial Triangulation. Helsinki 1994. 137 pages.
120. MARKKU POUTANEN (EDITOR): Interference measurements of the Taoyuan Standard Baseline. Helsinki 1995. 35 pages.
121. JORMA JOKELA: Interference measurements of the Chang Yang Standard Baseline in 1994. Kirkkonummi 1996. 32 pages.
122. OLLI JAAKKOLA: Quality and automatic generalization of land cover data. Kirkkonummi 1996. 39 pages.
123. MATTI OLLIKAINEN: Determination of orthometric heights using GPS levelling. Kirkkonummi 1997. 143 pages.
124. TIINA KILPELÄINEN: Multiple Representation and Generalization of Geo-Databases for Topographic Maps. Kirkkonummi 1997. 229 pages.
125. JUSSI KÄÄRIÄINEN AND JAAKKO MÄKINEN: The 1979-1996 gravity survey and the results of the gravity survey of Finland 1945-1996. Kirkkonummi 1997. 24 pages. 1 map.
126. ZHITONG WANG: Geoid and crustal structure in Fennoscandia. Kirkkonummi 1998. 118 pages.
127. JORMA JOKELA AND MARKKU POUTANEN: The Väisälä baselines in Finland. Kirkkonummi 1998. 61 pages.
128. MARKKU POUTANEN: Sea surface topography and vertical datums using space geodetic techniques. Kirkkonummi 2000. 158 pages
129. MATTI OLLIKAINEN, HANNU KOIVULA AND MARKKU POUTANEN: The Densification of the EUREF Network in Finland. Kirkkonummi 2000. 61 pages.
130. JORMA JOKELA, MARKKU POUTANEN, ZHAO JINGZHAN, PEI WEILI, HU ZHENYUAN AND ZHANG SHENGSHU: The Chengdu Standard Baseline. Kirkkonummi 2000. 46 pages.
131. JORMA JOKELA, MARKKU POUTANEN, ZSUZSANNA NÉMETH AND GÁBOR VIRÁG: Remeasurement of the Gödöllö Standard Baseline. Kirkkonummi 2001. 37 pages.
132. ANDRES RÜDJA: Geodetic Datums, Reference Systems and Geodetic Networks in Estonia. Kirkkonummi 2004. 311 pages.
133. HEIKKI VIRTANEN: Studies of Earth Dynamics with the Superconducting Gravimeter. Kirkkonummi 2006. 130 pages.
134. JUHA OKSANEN: Digital elevation model error in terrain analysis. Kirkkonummi 2006. 142 pages. 2 maps.
135. MATTI OLLIKAINEN: The EUVN-DA GPS campaign in Finland. Kirkkonummi 2006. 42 pages.
136. ANNU-MAARIA NIVALA: Usability perspectives for the design of interactive maps. Kirkkonummi 2007. 157 pages.
137. XIAOWEI YU: Methods and techniques for forest change detection and growth estimation using airborne laser scanning data. Kirkkonummi 2007. 132 pages.
138. LASSI LEHTO: Real-time content transformations in a WEB service-based delivery architecture for geographic information. Kirkkonummi 2007. 150 pages.
139. PEKKA LEHMUSKOSKI, VEIKKO SAARANEN, MIKKO TAKALO AND PAAVO ROUHIAINEN: Suomen Kolmannen tarkkavaaituksen kiintopisteluettelo. Bench Mark List of the Third Levelling of Finland. Kirkkonummi 2008. 220 pages.
140. EIJA HONKAVAARA: Calibrating digital photogrammetric airborne imaging systems using a test field. Kirkkonummi 2008. 139 pages.
141. MARKKU POUTANEN, EERO AHOKAS, YUWEI CHEN, JUHA OKSANEN, MARITA PORTIN, SARI RUUHELA, HELI SUURMÄKI (EDITORS): Geodeettinen laitos – Geodetiska Institutet – Finnish Geodetic Institute 1918–2008. Kirkkonummi 2008. 173 pages.

142. MIKA KARJALAINEN: Multidimensional SAR Satellite Images – a Mapping Perspective. Kirkkonummi 2010. 132 pages.
143. MAARIA NORDMAN: Improving GPS time series for geodynamic studies. Kirkkonummi 2010. 116 pages.
144. JORMA JOKELA AND PASI HÄKLI: Interference measurements of the Nummela Standard Baseline in 2005 and 2007. Kirkkonummi 2010. 85 pages.
145. EETU PUTTONEN: Tree Species Classification with Multiple Source Remote Sensing Data. Kirkkonummi 2012. 162 pages.
146. JUHA SUOMALAINEN: Empirical Studies on Multiangular, Hyperspectral, and Polarimetric Reflectance of Natural Surfaces. Kirkkonummi 2012. 144 pages.
147. LEENA MATIKAINEN: Object-based interpretation methods for mapping built-up areas. Kirkkonummi 2012. 210 pages.
148. LAURI MARKELIN: Radiometric calibration, validation and correction of multispectral photogrammetric imagery. Kirkkonummi 2013. 160 pages.
149. XINLIAN LIANG: Feasibility of Terrestrial Laser Scanning for Plotwise Forest Inventories. Kirkkonummi 2013. 150 pages.
150. EERO AHOKAS: Aspects of accuracy, scanning angle optimization, and intensity calibration related to nationwide laser scanning. Kirkkonummi 2013. 124 pages.
151. LAURA RUOTSALAINEN: Vision-Aided Pedestrian Navigation for Challenging GNSS Environments. Kirkkonummi 2013. 180 pages.
152. HARRI KAARTINEN: Benchmarking of airborne laser scanning based feature extraction methods and mobile laser scanning system performance based on high-quality test fields. Kirkkonummi 2013. 346 pages.
153. ANTERO KUKKO: Mobile Laser Scanning – System development, performance and applications. Kirkkonummi 2013. 247 pages.
154. JORMA JOKELA: Length in Geodesy – On Metrological Traceability of a Geospatial Measurand. Kirkkonummi 2014. 240 pages.
155. PYRY KETTUNEN: Analysing landmarks in nature and elements of geospatial images to support wayfinding. Kirkkonummi 2014. 281 pages.
156. MARI LAAKSO: Improving Accessibility for Pedestrians with Geographic Information. Kirkkonummi 2014. 129 pages.

The name of the series has changed the 1st of January in 2015.

FGI Publications:

157. LINGLI ZHU: A pipeline of 3D scene reconstruction from point clouds. Kirkkonummi 2015. 206 pages.

Finnish Geospatial Research Institute FGI
Geodeetinrinne 2
FI-02430 Masala
Finland

www.fgi.fi